(4)

The University of Texas at Dallas
Center for Quantum Electronics
The Gamma-Ray Laser Project
Quarterly Report
July-September 1989

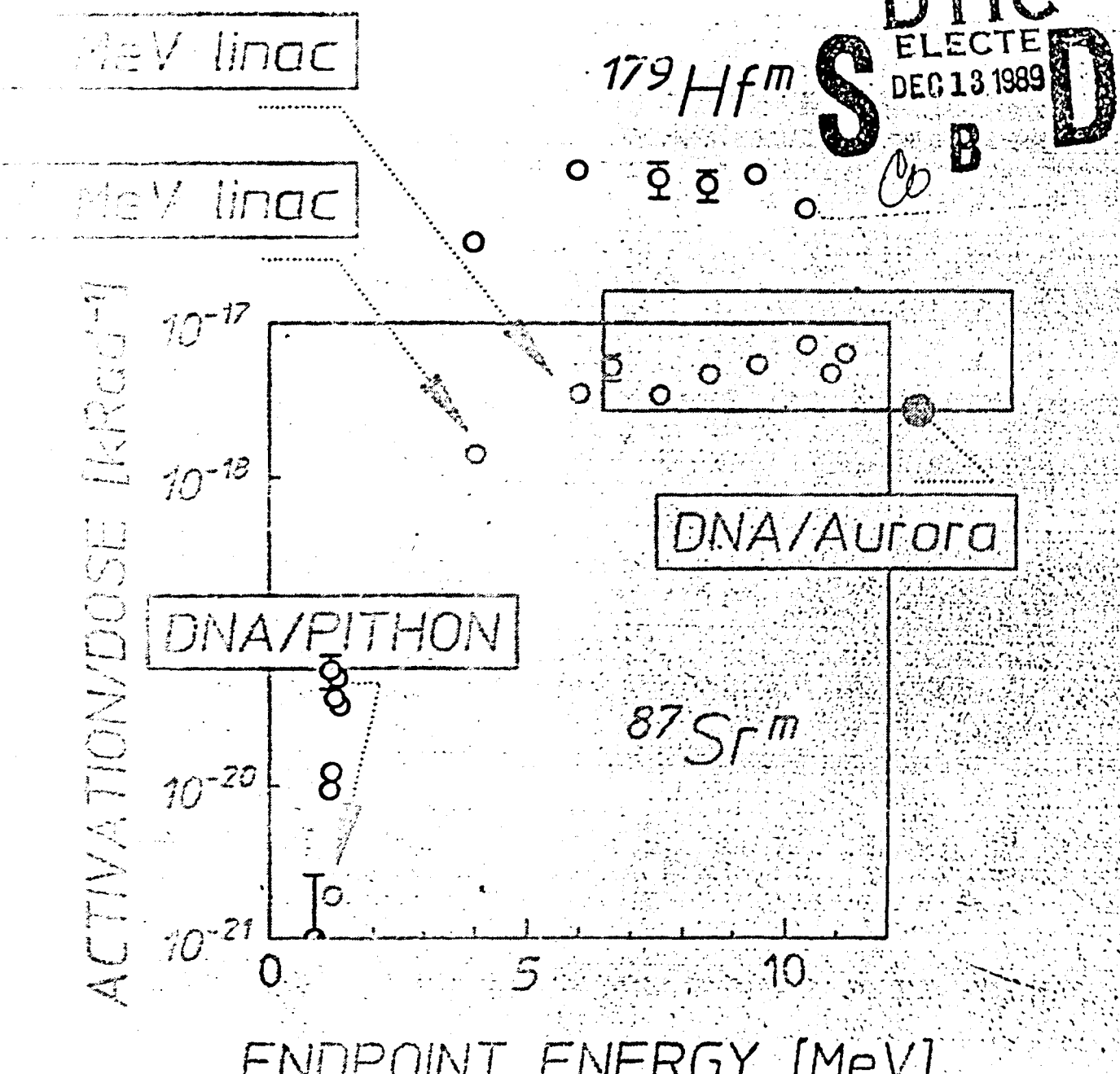

Report GRL/8902

PROOF OF THE FEASIBILITY OF COHERENT AND INCOHERENT SCHEMES FOR PUMPING A GAMMA-RAY LASER

Principal Investigator: Carl B. Collins
The University of Texas at Dallas
Center for Quantum Electronics
P.O. Box 830688
Richardson, Texas 75083-0688

October 1989

Quarterly Technical Progress Report
1 July 1989 through 30 September 1989
Contract Number N00014-86-C-2488

Prepared for
INNOVATIVE SCIENCE AND TECHNOLOGY DIRECTORATE
OF STRATEGIC DEFENSE INITIATIVE ORGANIZATION

Contracting Officer's Technical Representative
Dr. Paul Kepple, Code 4720
Naval Research Laboratory
4555 Overlook Avenue, SW
Washington, DC 20375-5000

SECURITY CLASSIFICATION OF THIS PAGE (When Data Entered)

REPORT DOCUMENTATION PAGE

READ INSTRUCTIONS BEFORE COMPLETING FORM

1. REPORT NUMBER: GRL/8902

2. GOVT ACCESSION NO.:

3. RECIPIENT'S CATALOG NUMBER:

4. TITLE (and Subtitle): PROOF OF THE FEASIBILITY OF COHERENT AND INCOHERENT SCHEMES FOR PUMPING A GAMMA-RAY LASER

5. TYPE OF REPORT & PERIOD COVERED: Quarterly Technical Progress 07/01/89 - 09/30/89

6. PERFORMING ORG. REPORT NUMBER:

7. AUTHOR(s): C. B. COLLINS

8. CONTRACT OR GRANT NUMBER(s): N00014-86-C-2488

9. PERFORMING ORGANIZATION NAME AND ADDRESS:
University of Texas at Dallas
Center for Quantum Electronics
P.O. Box 830688
Richardson, TX 75083-0688

10. PROGRAM ELEMENT, PROJECT, TASK AREA & WORK UNIT NUMBERS:

11. CONTROLLING OFFICE NAME AND ADDRESS:
INNOVATIVE SCIENCE AND TECHNOLOGY DIRECTORATE
OF STRATEGIC DEFENSE INITIATIVE ORGANIZATION

12. REPORT DATE: October 1989

13. NUMBER OF PAGES: 54

14. MONITORING AGENCY NAME & ADDRESS (if different from Controlling Office):
Dr. Paul Kepple
Naval Research Laboratory, Code 4720
4555 Overlook Avenue, SW
Washington, DC 20375-5000

15. SECURITY CLASS. (of this report): Unclassified

15a. DECLASSIFICATION/DOWNGRADING SCHEDULE:

16. DISTRIBUTION STATEMENT (of this Report)

This document has been approved for public release and sale; its distribution is unlimined.

17. DISTRIBUTION STATEMENT (of the abstract entered in Block 20, if different from Report)

18. SUPPLEMENTARY NOTES

19. KEY WORDS (Continue on reverse side if necessary and identify by block number)

20. ABSTRACT (Continue on reverse side if necessary and identify by block number)

Recent approaches to the problem of the gamma-ray laser have focused upon upconversion techniques in which metastable nuclei are pumped with long wavelength radiation. At the nuclear level the storage of energy can approach tera-Joules (10^{12}J) per liter for thousands of years. However, any plan to use such a resource for a gamma-ray laser poses

(continued on next page)

DD FORM 1 JAN 73 1473 EDITION OF 1 NOV 65 IS OBSOLETE
S/N 0102-LF-014-6601

SECURITY CLASSIFICATION OF THIS PAGE (When Data Entered)

20. Abstract (continued)

problems of a broad interdisciplinary nature requiring the fusion of concepts taken from relatively unrelated field of physics. Our research group has described several means through which this energy might be coupled to the radiation fields with cross sections for stimulated emission that could reach 10^{-17} cm^2. Such a stimulated release could lead to output powers as great as 3×10^{21} Watts/liter. Since 1978 we have pursued an approach for the upconversion of longer wavelength radiation incident upon isomeric nuclear populations that can avoid many of the difficulties encountered with traditional concepts of single photon pumping. Recent experiments have confirmed the general theory and have indicated that a gamma-ray laser is feasible if the right combination of energy levels and branching ratios exists in some real material. Of the 1,886 distinguishable nuclear materials, the present state-of-the-art has been adequate to identify 29 first-class candidates, but further evaluation cannot proceed without remeasurements of nuclear properties with higher precision. A laser-grade database of nuclear properties does not yet exist, but the techniques for constructing one have been developed under this contract and are now being utilized. Resolution of the question of the feasibility of a gamma-ray laser now rests upon the determination of: 1) the identity of the best candidate, 2) the threshold level of laser output, and 3) the upconversion driver for that material.

This quarter's report focuses upon our most recent efforts to cross calibrate our results from x-ray pumping with literature values of nuclear parameters. The exciting levels of fluorescence obtained in the course of recent experiments have been of such unexpected magnitude that the need has been perceived for a primary norm with which to tie present values to the paucity of measurements reported in the literature. Such a benchmark has been found in ^{87}Sr. In the course of work reported here, four accelerators were used in different environments at geographically separated sites to excite the reaction $^{87}Sr(\gamma,\gamma')^{87}Sr^m$. Absolute measurements of yield agreed completely, despite the wide range of possibilities for variances of spurious effects between the four systems. Moreover, all excitations produced by the different bremsstrahlung spectra with endpoints up to 4MeV could be explained precisely by a model of photoexcitation using only values of nuclear parameters established in the literature for more than 20 years. Under these same conditions, the nineteen isotopes showing g[illegible] resonances for pumping isomers still displayed the same extraordina[illegible] alues of integrated cross sections reported earlier. *As usual with [illegible]e experiments, no significant contributions were made by spurious neutrons evaporated from environmental materials.*

TABLE OF CONTENTS

PREFACE i

PHOTOEXCITATION OF NUCLEAR ISOMERS
BY (γ,γ') REACTIONS
by J. J. Carroll, M. J. Byrd, D. G. Richmond, T. W. Sinor, K. N. Taylor, W. L. Hodge, Y. Paiss, C. D. Eberhard, J. A. Anderson, and C. B. Collins
University of Texas at Dallas

E. C. Scarbrough and P. P. Antich
University of Texas Southwestern Medical Center

F. J. Agee, D. Davis, G. A. Huttlin, K. G. Kerris, M. S. Litz, and D. A. Whittaker
Aurora Simulator Facility, Harry Diamond Laboratory

Introduction 1
Methodology 6
Analytic Approach 6
Experimental Details 10
Results 24
Strontium as a Benchmark 24
Nuclide Survey 29
Neutron Excitations 34
Conclusions 43
References 46

PREFACE

Emphasis this quarter has continued to focus upon the successes enjoyed along the approach to the gamma-ray laser that depends upon incoherent pumping. Last year we had first reported the giant resonance for the dumping of the $^{180}Ta^{m}$ isomer by pumping samples with flash x-rays of relatively modest intensities from a 6 MeV linac in a scheme which is the nuclear analog of the ruby laser. This particular material, the worst of the 29 actual candidates, showed what was at that time the largest integrated cross section ever reported for interband transfer in any nuclear material, 4×10^{-22} cm^2 eV. This was an enormous value for bandwidth funneling to a fluorescent level, corresponding to about 0.5 eV of useful width for the absorption of the pump x-rays.

Studies we subsequently conducted showed that the giant pumping resonances occurred with a gratifying frequency throughout the table of nuclides. Concern had first arisen that these seemingly favorable structures might lie at high energies of excitation near the threshold for neutron evaporation, and so be associated in some way with the high density of nuclear states expected there. This has not proven to be the case. That particular experimental series culminated in a major milestone achievement in which *nineteen isomers were successfully pumped with the bremsstrahlung from a 4 MeV linac*. The density of nuclear states near 4 MeV should be exponentially reduced from values expected near 6 MeV, and yet most isomers were excited with comparable efficiencies by linacs operated at the two energies. The two poorest of the 29 candidates for a gamma-ray laser, $^{180}Ta^{m}$ and $^{123}Te^{m}$, showed the least variation in excitation when the end point of the bremsstrahlung was lowered from 6 to 4 MeV. Still, no other candidates are available, but results for these two would encourage expectations that the great width associated with pumping candidate isomers is concentrated at relatively few discrete transition energies.

The most recent efforts have been applied to a cross calibration of our photoexcitation results with literature values of nuclear parameters. The exciting levels of fluorescence obtained in the course of recent experiments have been of such unexpected magnitude that the need has been perceived for a primary norm with which to tie present values

to the paucity of measurements reported in the literature. Such a benchmark has been found in ^{87}Sr. In the course of work reported here, four accelerators were used in different environments at geographically separated sites to excite the reaction $^{87}Sr(\gamma,\gamma')^{87}Sr^{m}$. Absolute measurements of yield agreed completely, despite the wide range of possibilities for variances of spurious effects between the four systems. Moreover, all excitations produced by the different bremsstrahlung spectra with endpoints up to 4 MeV could be explained precisely by a model of photoexcitation using only values of nuclear parameters established in the literature for more than 20 years. Under these same conditions, the nineteen isomers showing giant resonances for pumping isomers still displayed the same extraordinary values of integrated cross sections reported earlier. *As usual with these experiments, no significant contributions were made by spurious neutrons evaporated from environmental materials.*

As has been the case since 1982, there are still no known factors which inhibit the realization of a gamma-ray laser. Neither the level of pump fluence required for laser threshold nor the waste heat to reject presents any particular problem in idealized materials. *A gamma-ray laser is feasible if the right combination of energy levels occurs in some real material.* When actually tested, the two poorest of the 29 candidate nuclei did surprisingly well, performing 1,000 to 10,000 times better than expected. The overriding question in resolving the feasibility of the nuclear analog to the ruby laser is whether or not one of the better of the 29 has its isomeric level in a position sufficiently near the ideal.

Continuing the preparation of this report as an "in-house" journal, this series presents material to reflect the individual contributions of the teams of research faculty and graduate students involved in these phases of the research. In this regard, I wish to thank all our staff for their splendid efforts in supporting the preparation of these manuscripts to a rather demanding timetable.

- C. B. Collins
- Director
- Center for Quantum Electronics

N00014-86-C-2488
UTD #24522-964

PHOTOEXCITATION OF NUCLEAR ISOMERS BY (γ,γ') REACTIONS

by J. J. Carroll, M. J. Byrd, D. G. Richmond, T. W. Sinor, K. N. Taylor, W. L. Hodge, Y. Paiss, C. D. Eberhard, J. A. Anderson, and C. B. Collins

E. C. Scarbrough and P. P. Antich
The University of Texas Southwestern Medical Center at Dallas

F. J. Agee, D. Davis, G. A. Hutlin, K. G. Kerris, M. S. Litz, and D. A. Whittaker
Aurora Simulator Facility, Harry Diamond Laboratories

INTRODUCTION

Because the photon carries relatively little momentum, (γ,γ') reactions must proceed through resonant channels for excitation with rather narrow widths. This aspect distinguishes photoexcitation from related processes such as (γ,n). The generation of an additional particle with which to conserve momentum provides a threshold of energy above which all incident photons can mediate the reaction. This facilitates the study of processes such as (γ,n) by increasing product yields and richly detailed results have been reported in the literature.[1] In contrast, the difficulties in exciting the narrow resonances through which (γ,γ') reactions must proceed have inhibited investigations and relatively few results have been published in the past 50 years over which such processes have been known.[2,3]

In the region of energies from 0.1 to 11.0 MeV photon sources are either fixed in energy or continuous in nature and the opportunity to probe (γ,γ') reactions with a tunable source of narrow width does not exist at practical levels of intensity. Generally experiments have been done with continua either intentionally, or unavoidably because of the degradation of line spectra by Compton scattering in actual geometries in which γ-sources are employed.

If threshold phenomena are being investigated, results are sensitive only to the integrals of the illuminating spectra as functions of energy and impressive precision can be achieved in the reaction cross sections finally reported.[1] Conversely, (γ,γ') reactions which must be excited through narrow windows of energy, depend upon details of the spectra of input intensities. Since the width of the reaction is usually much less than the scale over which any significant variations of intensity can occur, results are reported in terms of the integrated cross sections, $(\sigma\Gamma)_f$

$$(\sigma\Gamma)_f = \int_{\text{width}} \sigma_f(E)\, dE \quad , \tag{1}$$

where Γ is the width of the reaction channel, $\sigma_f(E)$ is the cross section for exciting the product state, f, and E is the energy of the incident photon.

The yield of such a (γ,γ') reaction will depend upon the product $I(E)(\sigma\Gamma)_f$, where I(E) is the spectral density of the irradiation in units such as photons/cm^2-keV. Thus, the accuracy in reporting integrated cross sections can be no better than the state of knowledge of I(E). The difficulties in characterizing such spectra have provided for decades of critical controversy.

The most tractable (γ,γ') reactions for study are those for the photoexcitation of isomeric states. These live long enough to be readily examined after termination of the input irradiation with its high level of concomitant noise. The archetypical case has been the reaction $^{111}Cd(\gamma,\gamma')^{111}Cd^m$. Three of the most recent measurements of the integrated cross section, $\sigma\Gamma$ were conducted in 1979, 1982, and 1987 with results of 35, 5.8, and 14 as reported in Refs. 4-6, respectively, in the usual units of 10^{-29} cm^2-keV. Probable errors were quoted as varying

only from 7 to 14% and yet, no two of the measurements were even within a factor of 2 of each other.

Recently, the technology has become available[7,8] to measure directly the spectrum of a source of pulsed bremsstrahlung, together with greatly improved computer codes[10] with which to calculate spectra expected in complex, but realistic geometries. These advances made it possible to resolve[11] the persisting controversies in the reaction $^{111}Cd(\gamma,\gamma')^{111}Cd^{m}$, as well as those[12] in $^{115}In(\gamma,\gamma')^{115}In^{m}$. As expected, it was found[11,12] that both $^{115}In^{m}$ and $^{111}Cd^{m}$ were excited by predominantly resonant absorption through intermediate states, called gateway states, near 1 MeV which were broadened by their relatively short lifetimes. The sharp onset of the (γ,γ') reactions with increasing energy relegated to less than 3% any contributions from non-resonant processes and indicated that the gateway states were reasonably well connected by radiative transitions to both the ground states and the isomers. It appears that the principle cause for the large discrepancy between previous measurements was the difficulty in adequately characterizing the spectra of the irradiation, as mentioned above. This was particularly true for radioactive sources since all spectral contributions away from the resonance lines were necessarily due to Compton continua generated by environmentally sensitive radiation transport processes.

The model for the photoexcitation of isomeric nuclei confirmed in this recent work[11,12] is shown in Fig. 1. Only two gateway levels are drawn as examples and the number actually participating depends upon the sequence of energy levels and transition probabilities for the particular nucleus being considered. In the resolution of previous conflicts in ^{111}Cd and ^{115}In the values finally confirmed lay within the scatter of earlier measurements and generally conformed to expectations based upon nuclear parameters measured by other means.[13] However, when studies were extended to the deexcitation of an isomeric sample through the reverse of the sequence shown in Fig. 1, quite unexpected results were obtained[14] for the reaction $^{180}Ta^{m}(\gamma,\gamma')^{180}Ta$.

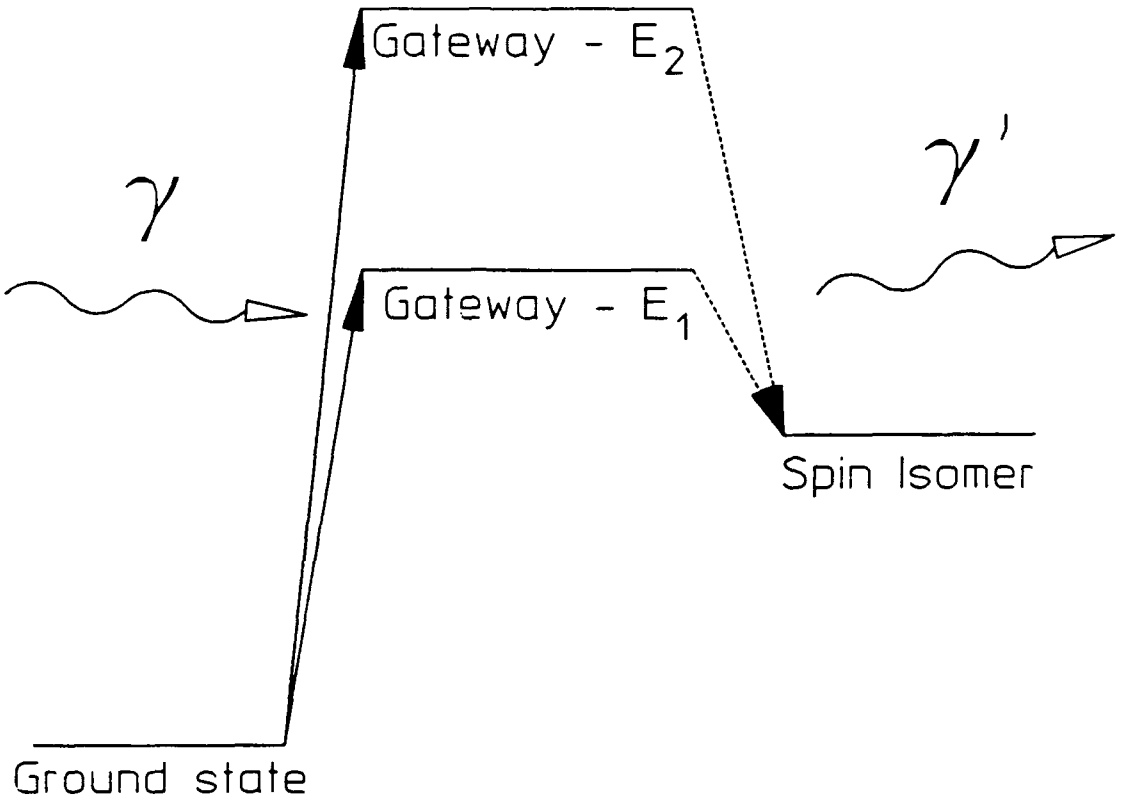

Figure 1: Schematic representation of the (γ,γ') reactions used to populate isomeric states in these experiments. The resonant absorption of bremsstrahlung x-rays denoted as γ, excite populations of gateway states. Two are shown at excitation energies of E_1 and E_2 but the actual number will vary for each nuclide. Parts of the populations of the gateway states make transitions to the final state either directly or as part of a cascade of radiative transitions ending on the final state as indicated by the dashed arrows.

The isomer $^{180}Ta^{m}$ is nature's rarest naturally occurring isotope.[15] Requiring an unlikely change of $\Delta J = 8$, the isomer was dumped to the ground state by bremsstrahlung having an endpoint of about 6 MeV. The partial width for this reaction was found[14] to be at least 0.5 eV, an enormous value exceeding any previous reports for (γ,γ') reactions by two to three orders of magnitude. The amount of deexcitation of the isomer observed was astonishing, corresponding to a total integrated cross section in excess of 4×10^{-25} cm^2-keV. This strength of the dumping reaction $^{180}Ta^{m}(\gamma,\gamma')^{180}Ta$ was qualitatively confirmed[16] with bremsstrahlung from the injector to the Darmstadt superconducting electron machine operated at 4.6 MeV. In this work the extension of these results to endpoint energies as low as 4.0 MeV will be described. Even more recently the reaction $^{176}Lu(\gamma,\gamma')^{176}Lu^{m}$ was reported to proceed with an integrated cross section of comparable magnitude.[17]

It was the purpose of the work reported here to examine the systematics of these giant resonances for the photoexcitation of isomeric states to determine whether such results were curiosities associated only with ^{176}Lu and $^{180}Ta^{m}$ or whether they were part of a more generally prevalent phenomena. To the extent possible it was intended to try to learn whether the large integrated cross sections were the results of a large number of reaction channels of more conventional size or rather, a few of unprecedented magnitude.

Unfortunately, the type of continuously variable electron accelerators that provided bremsstrahlung spectra with endpoint energies that could be selected in classical investigations[18] of (γ,γ') reactions is no longer available. For the experiments reported here we could arrange access only to a combination of accelerators, some with limited variability of endpoint energies such as DNA/PITHON at Physics International and DNA/Aurora at Harry Diamond Laboratories. Additional capabilities were contributed by two medical Linacs having fixed endpoint energies of 4 and 6 MeV. This enabled us to examine the photoexcitation of 19 isomeric nuclei, most of them over the full range from 0.5 to 11 MeV. The diversity of accelerators and locations contributed an operational benefit by tending to minimize the possibility of inadvertently introducing any systematic bias which might have been associated with any particular machine or its environment.

METHODOLOGY

Analytic Approach

The probability P(i -> f) that a nucleus undergoes a transition from the state i to the state f due to an x-ray exposure is the sum of the interaction probabilities for each (γ,γ') reaction which contributes to this process. This may be written as

$$P(i \rightarrow f) = \frac{N_f}{N_f} = \int_0^{E_{end}} \sigma(E) \frac{d\Phi(E)}{dE} dE , \qquad (2)$$

where N_f is the number of final states produced and N_i is a statistically large population of nuclei orginally in the state i. The irradiation is described by its endpoint energy E_{end}, and its spectral density $d\Phi(E)/dE$, or I(E), in photons/cm^2-keV. This is conveniently expressed as the product of the total photon flux Φ_o in photons/cm^2 and a relative spectral intensity function F(E) in keV^{-1} which is normalized according to the condition

$$\int_0^{E_{end}} F(E)\, dE = 1 , \qquad (3)$$

so that

$$\frac{d\Phi(E)}{dE} = I(E) = \Phi_o\, F(E) . \qquad (4)$$

In practice, the resonant gateways are sufficiently narrow in comparison to any features of the input spectra that Eq. (2) can be simplified as suggested by Eq. (1),

$$\frac{N_f}{N_i} = \sum_j (\sigma\Gamma)_{fj} \frac{d\Phi(E_j)}{dE} . \qquad (5)$$

Here, E_j is the energy of the j^{th} gateway level mediating the transition and the summation includes all which lie below E_{end}. The symbol $(\sigma\Gamma)_{fj}$ represents the integrated cross section in cm^2-keV for production of

this final state through the j^{th} gateway and includes contributions from all cascades which lead to f.

The integrated cross section is often expressed as $(\pi b_a b_o \sigma_o \Gamma/2)_j$ where b_a and b_o are the branching ratios for decay from the gateway level to the initial and final states, respectively. The Γ_j represents the natural width of the j^{th} state, whose lifetime τ_j gives $\Gamma_j = h/\tau_j$, and so $(b_a b_o \Gamma)_j$ is the partial width for the transition. The quantity σ_o is the amplitude of the Breit-Wigner cross section for the absorption,

$$\sigma_o = \frac{\lambda^2}{2\pi} \frac{I_j + 1}{I_i + 1} \frac{1}{\alpha_p + 1}, \qquad (7)$$

where λ is the wavelength in cm of the γ-ray at the resonant energy, I_j and I_i are the nuclear spins of the gateway and initial states, and α_p is the internal conversion coefficient of the absorption transition.

The above general development could be applied to most of the nuclei studied in this work by identifying i and f with the ground state and the isomer, respectively. In this direction a transition is said to pump the isomeric population. One nucleus, that of the tantalum isotope ^{180}Ta, is naturally abundant as the isomer rather than the ground state which has a relatively short lifetime. In this instance the initial level is the isomer; the final level is the ground state and the transition is considered as dumping the isomeric population.

Each of the isomers pumped in this work was identified by the emission of signature photons[19] with the exception of $^{176}Lu^m$ which decayed by β^- emission, as described later. The yields of final state populations were determined from the numbers of counts, C, collected in the corresponding peaks in pulse height spectra. These raw data were then corrected in a standard manner for the photopeak detector efficiency, η, the fraction of fluorescence photons per decay, q, and the finite times of sample transport and counting, D_1. The latter factor used literature values of the half-lives.[19] It was also necessary to account for some attenuation of the fluorescence photons within the samples themselves because of absorption and scattering events. This effect was accomodated by a transparancy factor A which was determined by Monte-Carlo calculations made for each sample. These corrections were confirmed by comparing the activations obtained from targets containing identical

materials, but in different geometries. The number of isomers produced in an exposure was then calculated from the expression,

$$N_f = \frac{C}{D_1 q \eta A} \quad . \tag{8}$$

The definition of the term D_1 restricts the utility of Eq. (8) to photoexcitation which occurs at a particular instant in time. This is acceptable when considering exposures made with "flash" x-ray devices such as nuclear simulators since the durations of those pulses are extremely short compared to the lifetimes of the isomers.

A further modification was necessary to correct the number of isomers produced by continuously operating (cw) devices which generate a uniformly spaced series of flashes. Fortunately, in the linacs used in this work both the durations of individual pulses and the times between them were very short. Also, the numbers of nuclei excited by each flash were small relative to the total numbers of target nuclei. It was therefore only necessary to consider the decays of independent populations during the irradiation period. This was done by introducing another factor, D_2, into the denominator of Eq.(8) equal to the fraction of all isomers produced that survived until the end of the exposure. This allowed the quantity D_1 to be retained as previously defined. In this way the activations, N_f/N_i were quantitatively obtained from the experimental data.

Substituting Eq. (4) into Eq. (5) and dividing by Φ_o gives an expression for a type of excitation function,

$$\frac{N_f}{N_i \Phi_o} = \sum_j (\sigma\Gamma)_{fj} \, F(E_j) \quad . \tag{9}$$

which can be useful as a sensitive indication for the opening of (γ,γ') channels whenever photons of the requisite energies, E_j become available. A change of the endpoint energy, E_{end} of the bremsstrahlung spectrum modulates the spectral intensity function $F(E_j)$ in Eq. (9) at all of the important gateway energies, E_j. The largest effect in the excitation function occurs when E_{end} is increased from a value just below some gateway at $E_j = E_k$ to one exceeding it so that $F(E_k)$ varies from zero to some finite value. In earlier work[18] plots of quantities equivalent to Eq. (9) as functions of the endpoint energies of the

irradiating spectra showed very pronounced activation edges which appeared as sharp increases at the energies, E_j, corresponding to excitation of new gateways.

In the work reported here the ratios of activations, N_f/N_i to the irradiation doses were examined as functions of E_{end}. The relationships between dose which was measured directly, and Φ_0 which had to be derived from it depended upon F(E). The normalization to dose rather than Φ_0 was chosen to avoid any dependence of the features of the excitation function upon interpretative models. Unfortunately, the relatively coarse mesh onto which endpoint energies could be set prevented any precise definition of the energies at which activation edges occurred for most nuclei studied here. However, their existence was very clearly indicated in the data.

A useful guide to interpolation was constructed in a second level of analysis. Previous works had shown that the integrated cross sections of higher lying resonances are generally larger than those of lower energy states.[18] Therefore, the highest gateway below the endpoint tended to dominate the photoexcitation process. A reasonable estimate for that level, if one existed, was obtained from Eq. (9) by assuming that only a single state mediated the transition at some unknown gateway energy E, so that

$$(\sigma\Gamma) = \frac{N_f}{N_i \Phi_0 F(E)} \quad . \tag{10}$$

The effective cross section, $\sigma\Gamma$ determined in this way from data produced by irradiation with a single endpoint, E_{end} was not unique. Rather, it was a collection of possible values that depended upon the spectral intensity of the radiation at the energy the dominant gateway might be assumed to lie. Plotted as a curve, the locus of such values varied from a minimum at the energy for which F(E) was maximal to an unbounded asymptote as $E \rightarrow E_{end}$ and $F(E) \rightarrow 0$. These plots were of particular utility when several sets of such numbers were obtained from different endpoint exposures and were then examined together. In some cases the intersections of those loci suggested at about what energies dominant gateways might lie.

Experimental Details

Sample materials were exposed to photons having energies up to 1.5 MeV with the DNA/PITHON nuclear simulator at Physics International. This device was a flash x-ray source using a single transmission line pulsed by a Marx generator. Since the endpoint energy could be varied to some degree by changing the charging voltage of the Marx, photoexcitation from 0.5 to 1.5 MeV could be investigated with a resolution limited by the available endpoint energies. The samples were placed in front of a converter foil which terminated the transmission line and were aligned to face the photon flash. These were exposed in complex packages to activate many materials in each shot, an important detail since DNA\PITHON could be fired no more than hourly. All the sample packages were backed with Thermoluminescent Dosimeters (TLD's) to measure accurately the dosage which each target received.

The 1.5 to 6 MeV range was studied with two fixed endpoint medical linacs at the Department of Radiology of the University of Texas Southwestern Medical Center at Dallas. Irradiations with nominal 4 MeV bremsstrahlung were obtained with a Varian Clinac 4/100 linac which provided a dose rate of 200 rad(H_2O)/min at 101.2 cm from the converter target. Bremsstrahlung having a nominal endpoint of 6 MeV was obtained with a Varian Clinac 1800 linac operating in the 6 MeV mode. This device produced 400 rad(H_2O)/min at 101.5 cm from the converter target. For both machines, the dose rate was determined by in-line ion chambers whose calibrations can be directly traced to NIST. Samples were exposed in packages confined to the region of most uniform dose distribution. Therefore, TLD's were not used with these accelerators.

Irradiations in the 6 to 11 MeV range were provided with the DNA/Aurora nuclear simulator, the world's largest flash x-ray accelerator,[20] located at the Harry Diamond Laboratories. Powered by a Marx bank, photons were generated by converter foils which terminated four seperate transmission lines. These converged on a target volume of roughly 0.1 m^3 in which the photon field was most intense. Again, the Marx charging voltage was varied to provide irradiations with different endpoint bremsstrahlung. Samples were suspended within the high intensity spot and were backed by TLD's. These packages were oriented to face the centerline of the machine rather than any particular transmission line.

The spectra of these four machines have been well characterized, particularly the linacs which are committed to patient treatment. Photon spectra of the DNA/PITHON and DNA/Aurora accelerators were obtained through use of the Integrated TIGER Series (ITS) computational program.[10] This coupled electron-photon transport code is well documented and widely used in the flash x-ray community. Results obtained in this way are usually calibrated by matching the endpoint energy and the total dosage to the shape of the calculated spectrum. The DNA/PITHON device could also be cross-calibrated by the activation technique described in Refs. 7 and 8. Typical spectra are given in Fig. 2 which shows the relative intensity function F(E), on the meshes of energies for which data were available. For the DNA/PITHON shot shown, $\Phi_0 = 4 \times 10^{14}$ photons/cm^2 and for the DNA/Aurora shot, $\Phi_0 = 5 \times 10^{13}$ photons/cm^2.

The output spectra of the medical linacs employed in this work were calculated with the established EGS4 code developed at SLAC.[9] Unfortunately, the relative spectral intensity functions of these devices that were found in the literature[21] contained a computational artifact. To minimize that feature the spectra had to be modeled as part of this work. Results are shown in Fig. 3, together with the literature values for a typical case.[21] The total fluxes at 100 cm were 3.23×10^{11} photons/cm^2-min for the nominally 4 MeV device, and 5.35×10^{11} photons/cm^2-min for the Clinac 1800 in the 6 MeV mode.

The isotopes studied in these experiments are listed in Table I along with some relevant physical parameters. The techniques employed to obtain measurements of activation depended upon the lifetimes of the isomeric states and whether or not these were long enough to transport the irradiated samples by simple means.

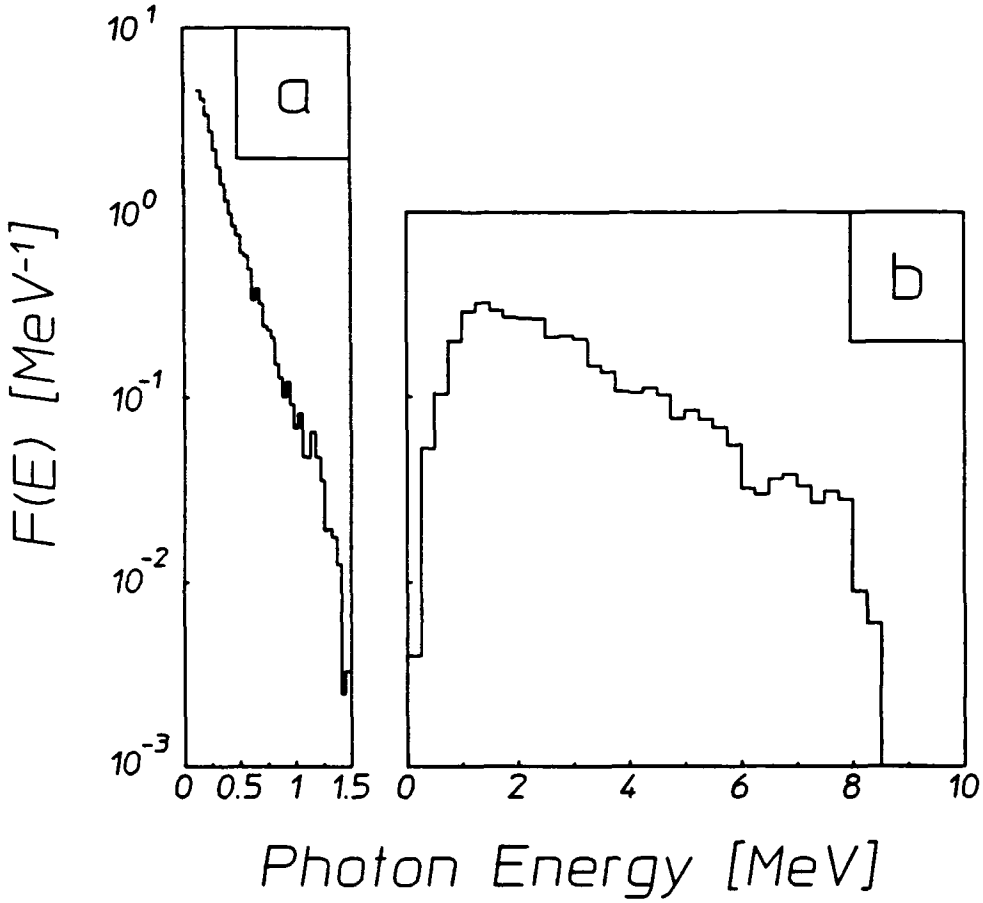

Figure 2: Relative spectral intensities, F(E) of the bremsstrahlung typically produced by nuclear simulators used to irradiate samples in these experiments. The curves are normalized so that the areas under the curves are unity. The devices employed were:
a) DNA/PITHON, with an endpoint of 1.5 MeV.
b) DNA/AURORA, with an endpoint of 8.5 MeV.

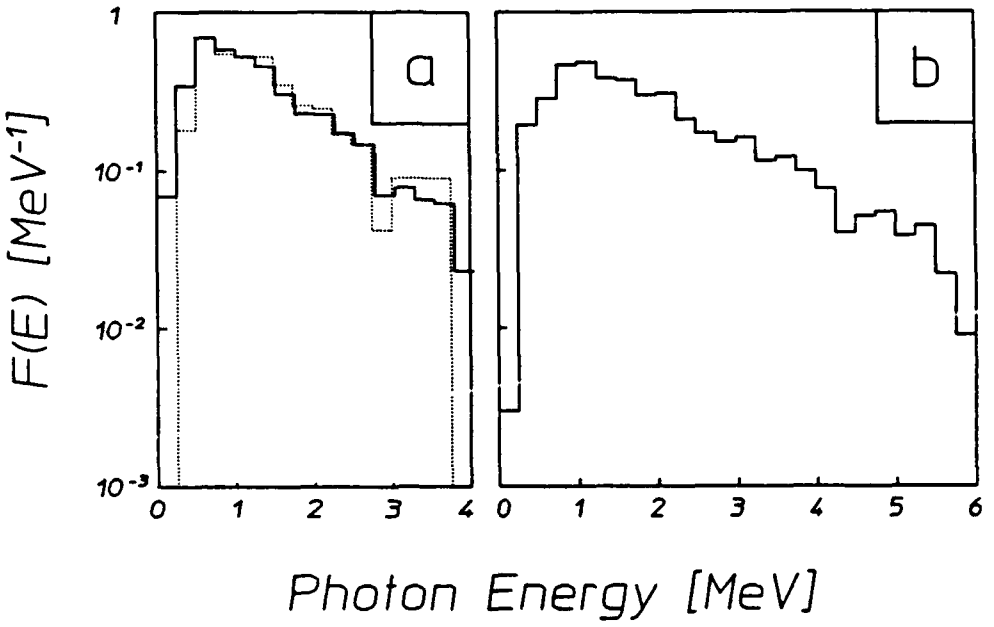

Figure 3: Relative spectral intensities, F(E) of the bremsstahlung produced by the medical linacs used to irradiate samples in these experiments. The curves are normalized so that the areas under the curves are unity. The solid lines indicate empirical fits to the calculated spectra as discussed in the text. The devices employed were:
a) Varian Clinac 4/100, with a nominal endpoint of 4 MeV. The dotted curve shows the spectrum obtained from Ref. 21 which contains a large spurious artifact at about 3 MeV.
b) Varian Clinac 1800, operated in the nominal 6 MeV enpoint mode.

*Table I. Summary of isomeric nuclei studied. Nuclei marked * were present in isotopically enriched samples. In the sample column, R refers to samples contained in rabbits, P to flat planchettes, F to metallic foils, and B to scintillation bottles. The ^{180}Ta sample consisted of a dusting of oxide on a thin aluminum plate, referred to by D. In the case of the ^{176}Lu sample, β^- particles were observed instead of fluorescence photons; the NA in the transparency column indicates that this factor was not applicable for ^{176}Lu.*

Nuclide	Abundance [%]	Sample Form	$T_{1/2}$	Principal Fluorescence [keV]	Transparency
^{167}Er	91.54 *	Er_2O_3 (R)	2.28 sec	207.79 (41.70%)	57.90
^{79}Br	50.69	LiBr (R)	4.86 sec	207.20 (75.80%)	84.90
^{191}Ir	37.30	Ir (R)	4.94 sec	129.43 (25.70%)	10.50
^{197}Au	100.00	Au (R)	7.80 sec	279.11 (73.00%)	92.70
^{89}Y	100.00	YF_3 (R)	16.06 sec	909.15 (99.14%)	94.70
^{77}Se	94.38	Se (R)	17.45 sec	161.92 (52.40%)	72.28
^{179}Hf	13.63	HfO_2 (R)	18.68 sec	214.31 (94.20%)	52.40
^{199}Hg	16.90	Hg_2Cl_2 (R)	43.20 sec	158.40 (53.00%)	43.96
^{137}Ba	11.74	BaF_2 (R)	153.12 sec	661.66 (90.10%)	95.50
^{111}Cd	12.80	Cd (F)	48.6 min	245.49 (94.00%)	76.35
^{113}In	4.30	In (F)	1.66 hr	391.69 (64.20%)	98.30
^{87}Sr	7.00	SrF_2 (P)	2.81 hr	388.40 (82.30%)	95.78
^{176}Lu	2.59	$LuCl_2$ (B)	3.63 hr	beta	NA
^{115}In	95.70	In (F)	4.49 hr	336.26 (45.80%)	98.00
^{180}Ta	4.00 *	TaO_2 (D)	8.15 hr	55.79 (36.00%)	100.00

^{135}Ba	6.60	BaF_2 (P)	1.20 d	268.27 (15.60%)	94.33
^{195}Pt	33.80	Pt (Coin)	4.02 d	98.88 (11.40%)	4.76
^{117}Sn	7.70	Sn (F)	13.6 d	158.56 (86.40%)	92.89
^{123}Te	0.908	Te (P)	119.7 d	158.99 (84.00%)	62.68

Isomers of the first nine nuclides listed in Table I have half-lives of less than three minutes and therefore required special treatment. These samples consisted of either powders or metallic foils enclosed in cylindrical polyethylene vials, termed rabbits, which were pneumatically transported to a well-type NaI(Tl) detector after exposure. The low energy resolution of this detector necessitated some care in the identification of the prominent features in the pulse height spectra. In all cases, confirmations that these were the fluorescence signatures of the isomers were made by determining the half-lives of the populations emitting these lines for comparision with literature values. This was made possible by simultaneously acquiring data through two Ortec 918A ADCAM multichannel buffers controlled by a personal computer. While one ADCAM served to produce a pulse height spectrum, the other collected a record of the total counts received in the preset dwell interval as a function of time. A typical example of the data obtained in this way is given in Figs. 4 and 5, showing measurements for the isomer $^{167}Er^{m}$.

The remaining nuclides in Table I were investigated in a less hurried, but similar fashion, with the exception of ^{176}Lu. The isomers of those nuclei have half-lives longer than 48.6 min, so they were transported by hand to a nearby solid-type Na(Tl) detector for counting. Samples containing particularly long-lived isomers like $^{123}Te^{m}$ ($T_{1/2}$ = 119.7 days) and $^{117}Sn^{m}$ ($T_{1/2}$ = 13.61 days) were transported to the Center for Quantum Electronics where they were counted using a high-purity, n-type germanium (HPGe) detector. The physical form of the materials in this slower class consisted either of thin metallic disks or metallic chips or chemical compounds contained within flat polyethylene planchettes.

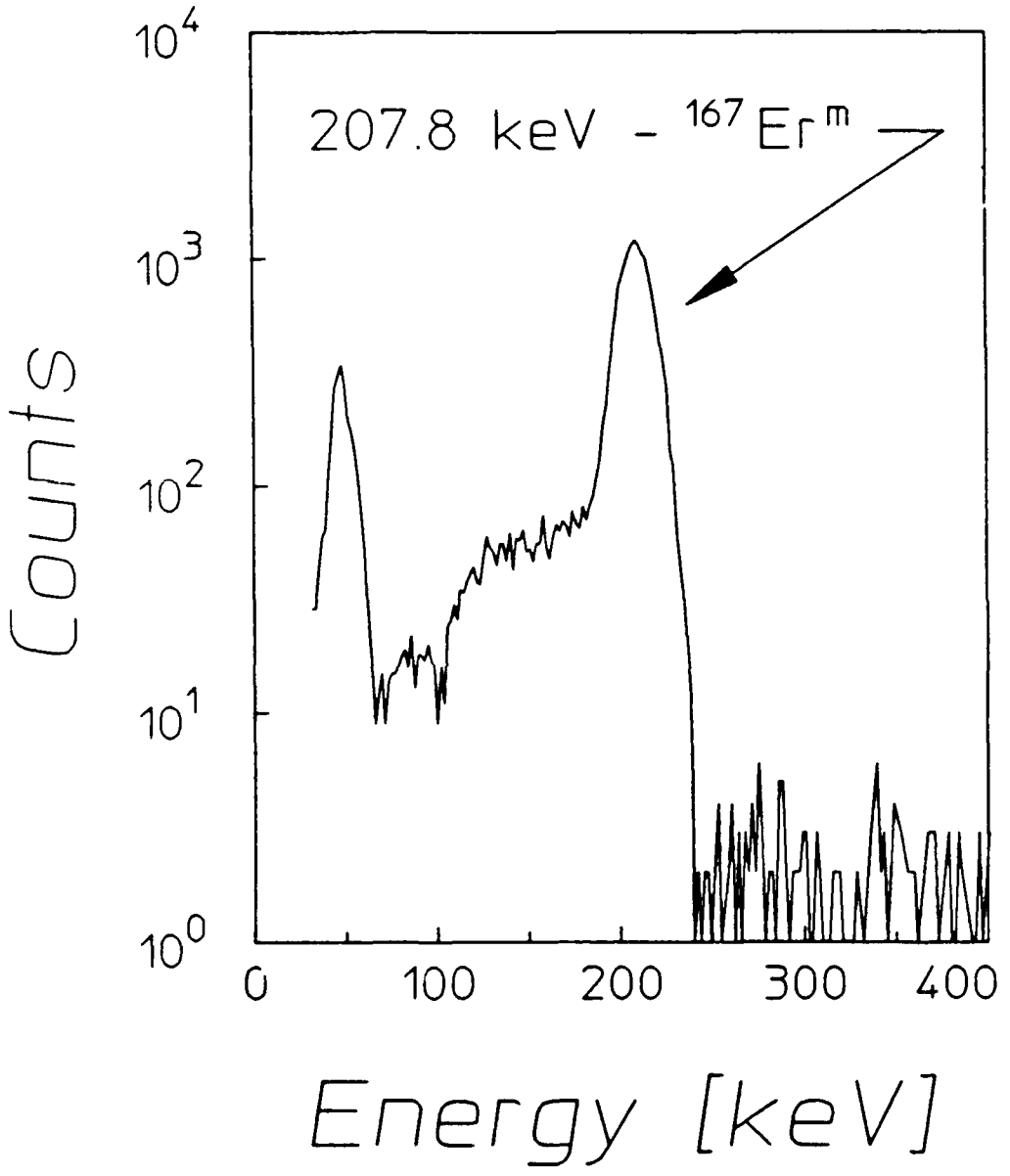

Figure 4: A typical pulse height spectrum showing the 207.8 keV fluorescence line from the decay of $^{167}Er^{m}$ following a 6 MeV exposure. The spectrum was obtained with a 7.6 cm × 7.6 cm diameter NaI(Tl) detector having a 5.1 cm × 2.5 cm diameter well. The sample was irradiated for 25 sec and the counting period was 5 sec in duration. The transport time from the end of irradiation to the start of counting was 2.06 sec.

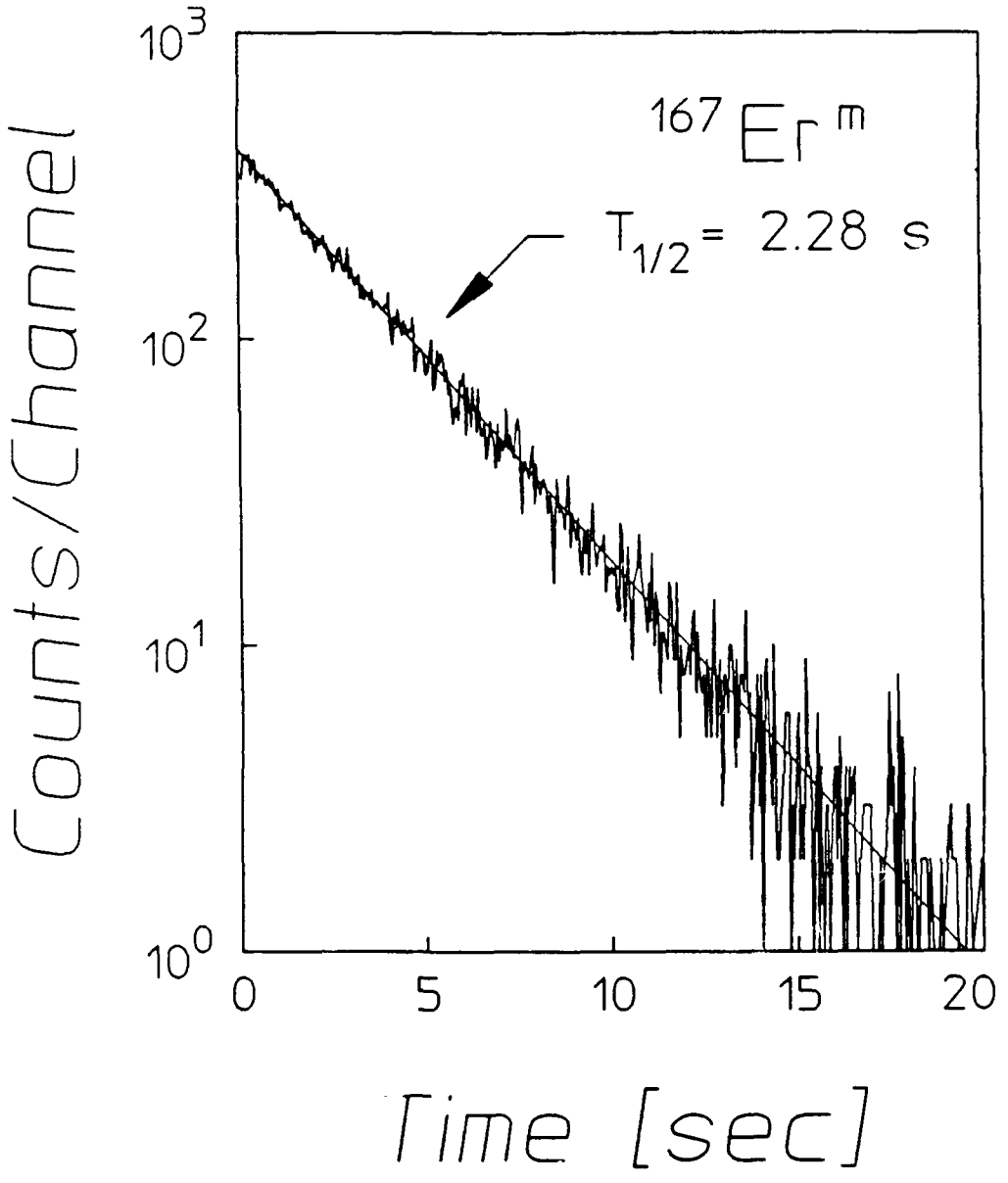

Figure 5. Data typical of the total counting rate measured for $^{167}Er^m$ as a function of the time elapsed from the start of the counting interval following a 6 MeV exposure. The solid line indicates the decay expected from the literature value of the half-life, 2.28 sec. The spectrum was obtained by recording the number of counts observed in successive dwell intervals of 0.05 sec with a multichannel scalar, and all events above a chosen lower level of discrimination were measured. The counting device was a 7.6 cm × 7.6 cm diameter NaI(Tl) detector having a 5.1 cm × 2.5 cm diameter well.

Since the HPGe detector provided greater resolution it was not so necessary to monitor the time decay in detail. For some samples however, energy spectra were acquired after several different elapsed times to provide additional confirmation of the signature identifying the product. This concern was exemplified in measurements of the isomer $^{123}Te^{m}$. A pulse height spectrum following a 6 MeV exposure is shown in Fig. 6. The fluorescence line at 159 keV is well defined and gives 5% counting statistics. This was rewarding since there was some concern that the activation might be hidden by the natural background of the counting chamber. Since this was the longest lived isomer ever reported to be excited by a (γ,γ') reaction, the time decay was experimentally determined from a sequence of energy spectra taken after a 6 MeV exposure. The decay of the count rate is shown in Fig. 7. A fit to this data gives a half-life which is in excellent agreement with the literature value.

The remaining nuclide, ^{176}Lu, was examined with a different detection scheme. The ground state of this isotope β^- decays with an endpoint energy of 565 keV and the isomer β^- decays with endpoint energies of 1313 keV (39.6%) and 1225 keV (60.4%). Since the isomer does not return to the ground state by a radiative transition, the number of excited nuclei must be measured by the detection of either β^- particles or the signature photons from the daughter nucleus. This type of deexcitation process is similar to that of ^{180}Ta, which decays by both electron capture and β^- modes.

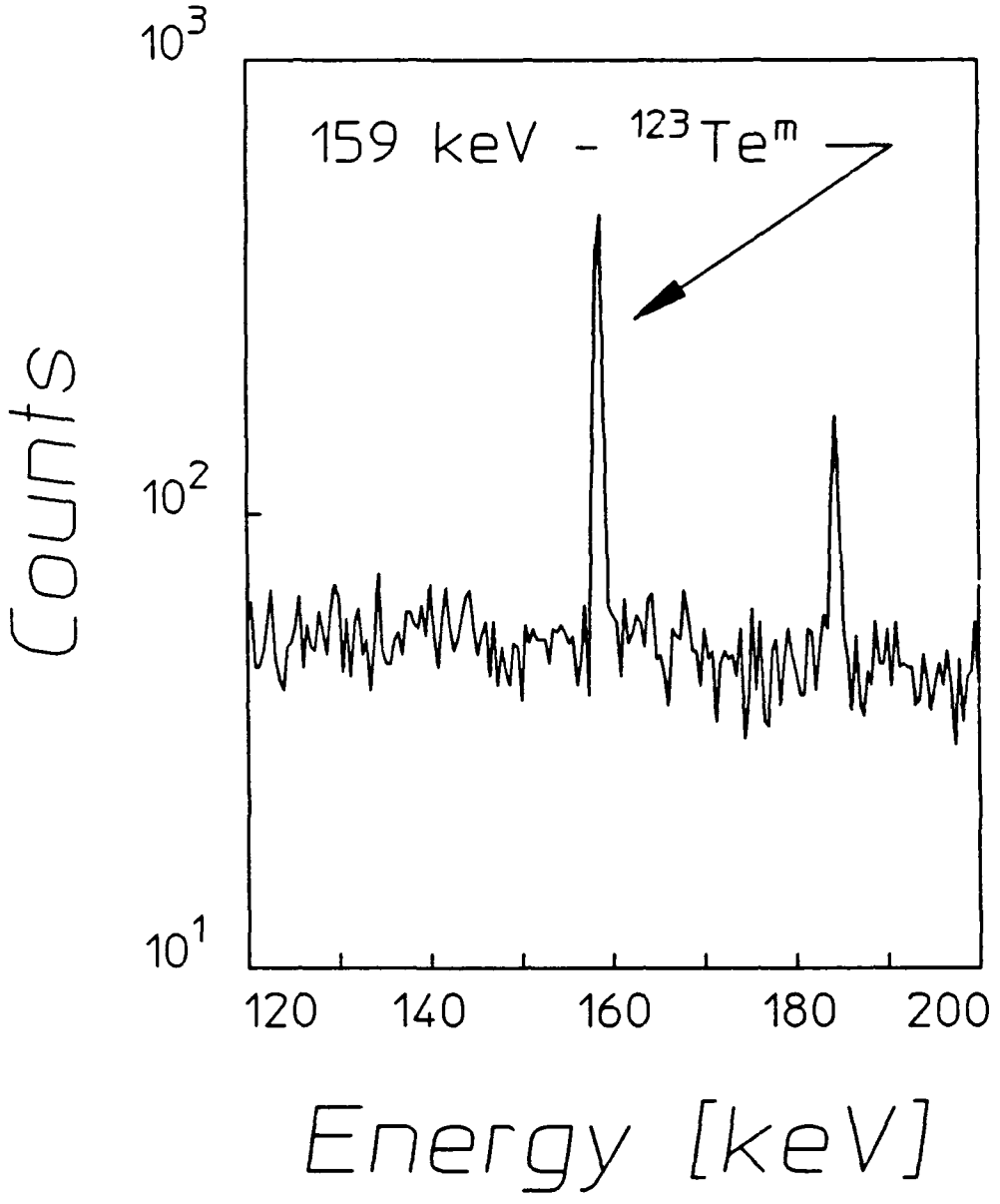

Figure 6: A typical pulse height spectra showing the 159 keV fluorescence line from the decay of $^{123}Te^m$ following a 6 MeV exposure. The spectrum was obtained with an n-type high purity germanium detector. The sample was irradiated for 2 hours and the counting period was 10 hours. The delay time from the finish of the irradiation to the beginning of the counting period was 22.98 hours.

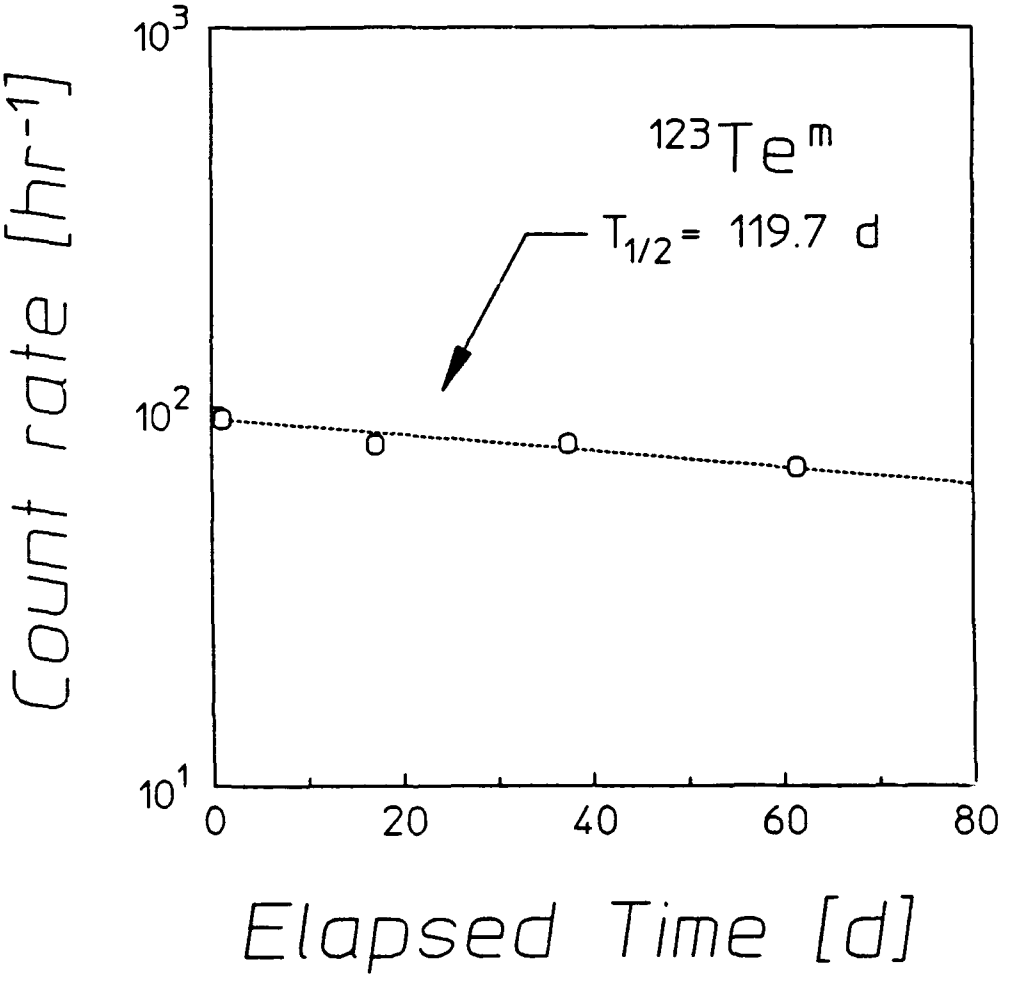

Figure 7: Plot of the time decay of the 159 keV fluorescence line from the decay of $^{123}Te^m$ following exposure to bremsstrahlung from the 6 MeV linac. The points represent the counting rate observed in several pulse height spectra performed at different elapsed times. The sizes of the symbols are comparable to one standard deviation and the counting periods were all 10 hours. The dashed line indicates the expected decay for a half-life of 119.7 days, taken from the literature, and is in good agreement with the measurements.

In the case of ^{176}Lu, the β^- decay energies allowed the use of a Cerenkov detector. Samples consisting of $LuCl_3$, dissolved in distilled water, were contained in polyethylene scintillation bottles. The Cerenkov threshold in water is about 250 keV and β^- particles emitted in the decay of the isomeric states were nearly 10 times more efficient in producing Cerenkov events than those emitted from ground state nuclei. Photons from these events were measured by a system consisting of two RCA 8850 photomultiplier tubes in EG&G bases. The tubes were used in a coincidence mode by connecting their time synchronized outputs through a 150 MHz Phillips 755 logic unit, thereby recongizing only coincident signals from the Cerenkov photons produced by single β^- particles. These output pulses were recorded as functions of elapsed time in multichannel scalar spectra where each channel represented a dwell time of 40 sec. The detector was calibrated with ^{40}K decays from a KCl solution of known activity, since the resulting β- particles had roughly the same endpoint energy as those from $^{176}Lu^m$. In these measurements, the individual count rates were monitored to avoid contributions from accidental coincidences triggered by separate β^- events or by thermoluminescence from the material of the bottle. A fit to the experimental data shown in the typical spectrum of Fig. 8 produced a value for the half-life for $^{176}Lu^m$ of 3.58 ± 0.05 hours, which was in good agreement with the literature value of 3.63 hours. The observed count rate was corrected back to the time immediately following the exposure and the number of isomers was determined as previously described.

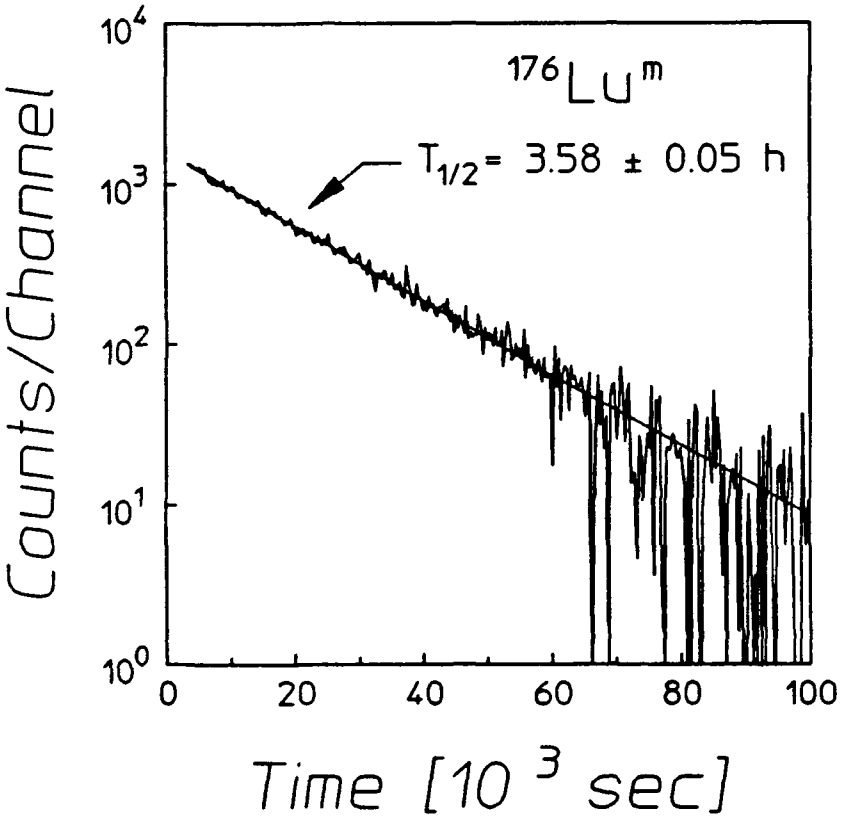

Figure 8: Data typical of the total counting rate measured for $^{176}Lu^{m}$ as a function of the time elapsed from the start of the counting interval following a 6 MeV exposure. This result was obtained by recording the number of counts observed in successive dwell time intervals of 320 sec with a multichannel scalar. The device used to make these measurements consisted of two RCA 8850 photomultiplier tubes operated in a coincidence mode as discussed in the text. The sample was irradiated for 40 minutes and the delay time from the finish of the irradiation to the beginning of the counting period was 53 minutes. A fit to the data is shown by the solid line and gives a half-life of 3.58 ± 0.05 hours, in good agreement with the literature value of 3.63 hours.

RESULTS

Strontium as a Benchmark

Normalized activation measurements obtained from all four accelerators for $^{87}Sr^{m}$ are shown in Fig. 9, which also indicates the threshold energy for (γ,n) reactions, E_n, at 8.428 MeV. The datum at 1.2 MeV represents an upper limit since no fluorescence photons were observed above the background level. Although lacking in resolution in the critical range from 1.2 to 6 MeV, the data allows several conclusions to be drawn about the photoexcitation process. Most important is that, even though the amount of normalized activation above 1.2 MeV is suprising, there is no evidence to support the significant participation of any non-resonant processes. This type of mechanism, if present, would be heavily dependent upon the density of nuclear states, which rises sharply at energies approaching E_n. The slow increase in the excitation function above 6 MeV relative to the change seen below 4 MeV would seem to preclude this as the dominant means of photoexcitation.

The large increase in normalized activation from 1.2 to 4 MeV indicates that at least one resonant gateway of significant magnitude lies in that range. The experimental resolution, however, does not allow a clear observation of the activation edges so the details of these states cannot be directly determined. Nevertheless, some inferences can be drawn from the plot of Fig. 10, which shows the effective integrated cross sections determined from both 4 and 6 MeV measurements as obtained from Eq. (10). The intersection near the 4 MeV asymptote implies that the two sets of data are the result of photoexcitations dominated by different gateways. Therefore, an additional gateway with an integrated cross section larger than any lying below 4 MeV must exist between 4 and 6 MeV.

Fortunately, the isomer $^{87}Sr^{m}$ is distinguished by the degree to which its photoexcitation has been characterized in the literature. An early work,[18] which used an x-ray source of the type no longer available, examined the production of this isomer by bremsstahlung with endpoints which could be varied up to 3 MeV. The tunability of that device allowed three distinct gateways to be identified at 1.22, 1.88, and 2.66 MeV, and their integrated cross sections to be measured. In the usual units of 10^{-29} cm^2-keV, these were found to be (8.5 + 4 - 3), (16 + 8 - 5) and (380 + 200 - 100), respectively.

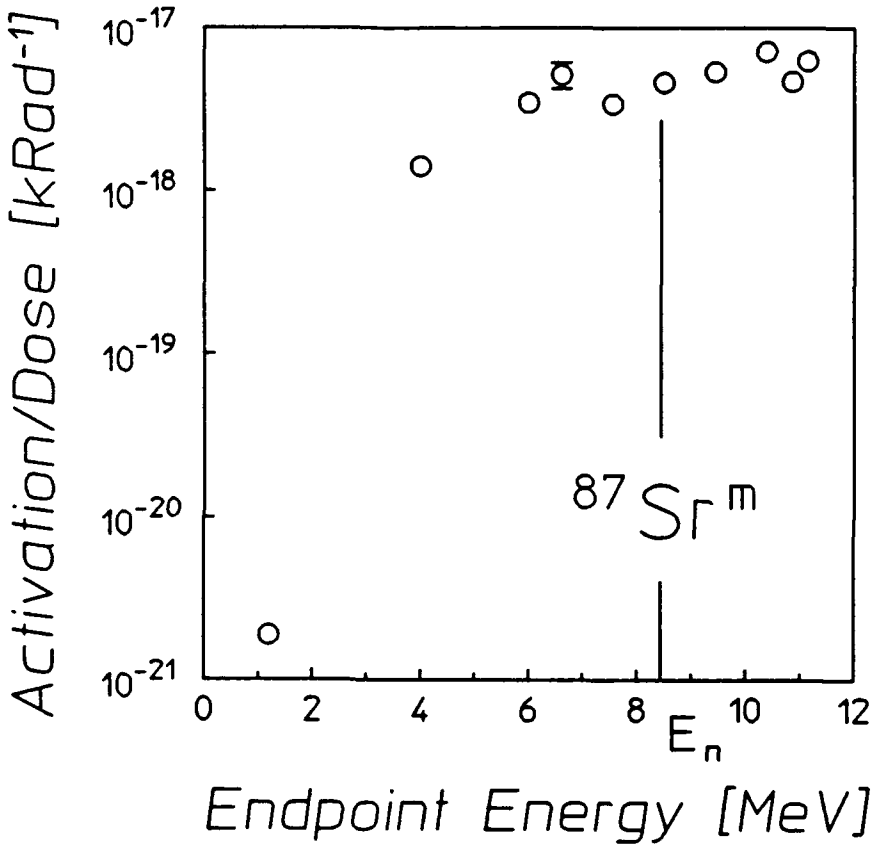

Figure 9: Normalized activation obtained from irradiations with all four accelerators for $^{87}Sr^{m}$. The size of the symbols is comparable to one standard deviation except where error bars are explicitly shown. The point at 1.2 MeV determined from a DNA/PITHON exposure is an upper bound on the excitation since no fluorescence photons were observed above the level of background. The vertical line indicates the neutron evaporation threshold at E_n = 8.4 MeV.

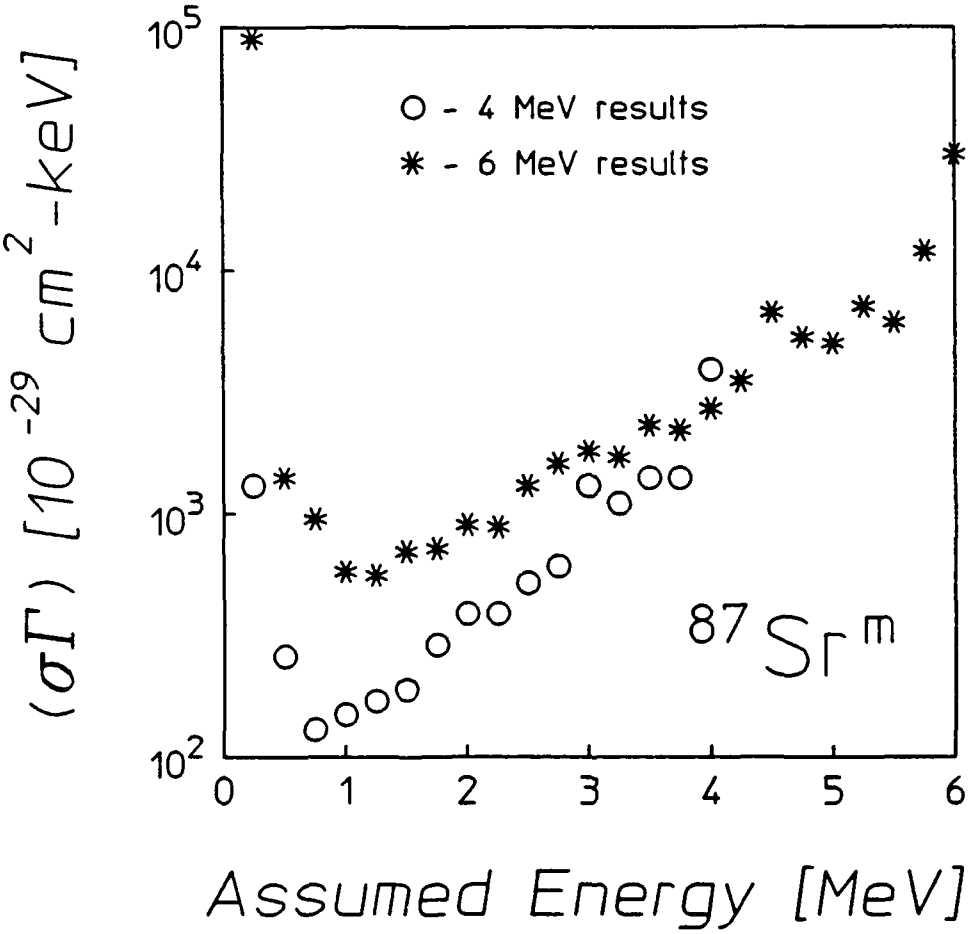

Figure 10: Integrated cross sections for the reaction $^{87}Sr(\gamma,\gamma')^{87}Sr^m$ through single, unknown gateway states as functions of the energies at which these states could be assumed to lie. The circles indicate the results of measurements using the 4 MeV linac while the asterisks show those from the 6 MeV experiments.

Figure 11a shows the ^{87}Sr data together with the normalized activations that should have been excited through the known gateways by photons with energies below 4 MeV. These values were calculated from Eq. (5) for many endpoint energies by using typical bremsstrahlung spectra scaled from those shown in Fig. 3. The composite graph produced in this way exhibits the required activation edges at 1.22 and 2.66 MeV in agreement with the actual measurements. No edge is apparent at 1.88 MeV, but this is due to the comparable magnitude and proximity of this level to the one at 1.22 MeV.

The correlation of the expected values near 4 MeV with the datum there indicates that no new states are required to explain all of the normalized activation obtained with the 4 MeV linac. This is in agreement with the preliminary conclusions reached by considering Fig. 9, as discussed above. Figure 10 gives an integrated cross section of 610×10^{-29} cm^2-keV for a single state lying between 2.5 and 2.75 MeV, only about one standard deviation above the known dominant level. Although this is an overestimation due to contributions of the other states, it is acceptable when compared to the literature value of $(380 + 200 -100) \times 10^{-29}$ cm^2-keV. This agreement is far better than that between the measurements of Refs. 4-6.

The data above 6 MeV in Figs. 9 and 11a significantly exceed the photoexcitation which could have been produced through the three known gateways. This extra activation must have therefore represented (γ,γ') reactions which proceeded through one or more unidentified levels. The simplest picture which matches the data is that of a single gateway near 5 MeV with an integrated cross section of the order of 4000×10^{-29} cm^2-keV. The normalized activation expected from this state, as well as those previouly identified, is shown in relation to the experimental data in Fig. 11b.

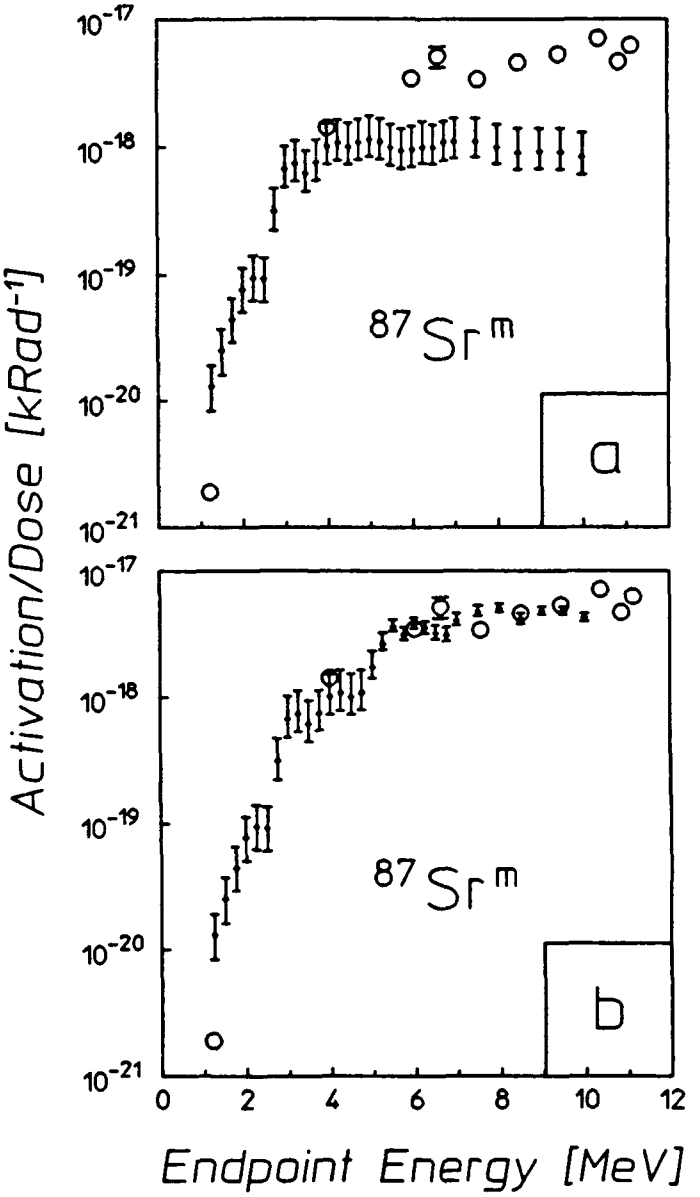

Figure 11: Normalized activation obtained from irradiations with all four accelerators for $^{87}Sr^{m}$ as previously shown in Fig. 9. Also displayed are excitation functions calculated from Eq. (5) for:
a) Expected photoexcitation through only the three known gateways of Ref. 18. The error bars indicate the uncertainties in the measurements of ($\sigma\Gamma$) in that work.
b) Expected photoexcitation through the three known gateways plus that of a hypothetical state near 5 MeV with integrated cross sections on the order of 4000 × 10^{-29} cm^2-keV. The error bars indicate only the uncertainties in the measured ($\sigma\Gamma$) of Ref. 18.

The nuclide ^{87}Sr provides a benchmark for other (γ,γ') studies since this is the only instance in which the current work can be compared with earlier experiments over a significant range of energies. It is rewarding that the present measurements of the photoexcitation of $^{87}Sr^{m}$ below 4 MeV are completely explained by resonant absorption of photons through gateways already reported in the literature.[18] The previous identification of these states has provided a means of validating the interpretive approach described above. Clearly, data as shown in Figs. 9 and 10 can give useful indications of the locations and integrated cross sections of participating resonances even when insufficient experimental resolution is available for a precise determination of these quantities.

Nuclide Survey

All of the nuclei of Table I were irradiated with the DNA/PITHON accelerator. The normalized activations we observed were generally on the order of 10^{-21} $krad^{-1}$, even after exposures made with bremsstralung having the highest available endpoint energy for that device. For most of the materials there was little variation in the normalized activations measured over a range of shots. Therefore, in the context of exploring the systematics of the larger resonances responsible for higher energy photoexcitations, these measurements are of limited usefulness. Although they cannot be employed to identify activation edges, they can serve to provide a baseline of activation below the onset of any of the giant gateways. A typical example of this utility is shown in Fig. 12 which displays data obtained for the isomer $^{167}Er^{m}$ along with those for $^{87}Sr^{m}$.

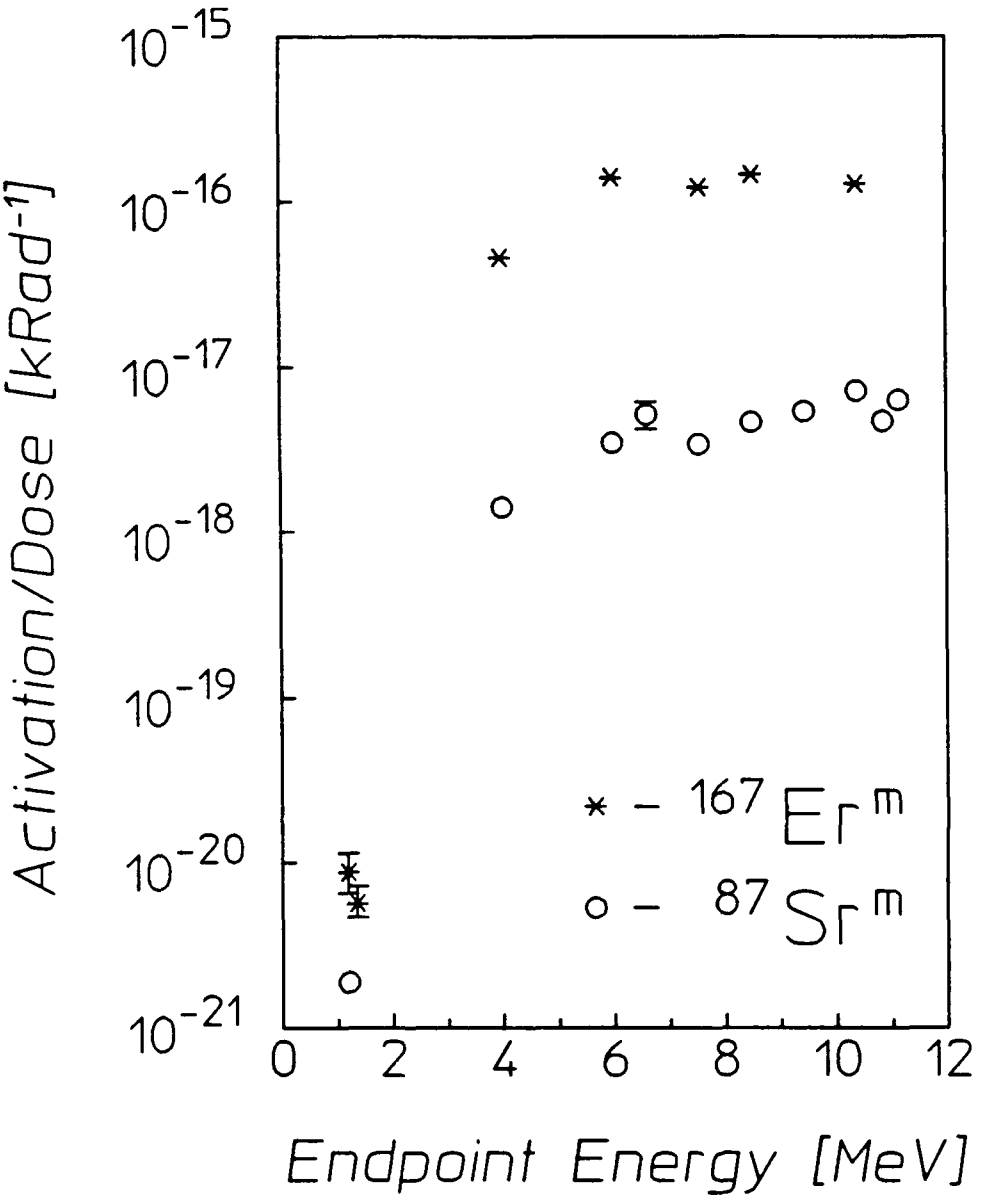

Figure 12: Normalized activation obtained from irradiations with all four accelerators for $^{167}Er^{m}$. Also included for the purpose of comparison are those values for $^{87}Sr^{m}$. The size of the symbols is comparable to one standard deviation except where error bars are explicitly shown. The point at 1.2 MeV determined from a DNA/PITHON exposure is an upper bound on the excitation since no fluorescence photons were observed above the level of background. The neutron evaporation thresholds are not indicated for ^{167}Er and ^{87}Sr, but are 6.4 and 8.4 MeV, respectively.

An examination of this plot indicates some interesting behavior. Although the normalized activation achieved with ^{167}Er nuclei is nearly two orders of magnitude larger than that of the ^{87}Sr benchmark, both isomers display similarly slow increases in activation above 6 MeV. This is surprising since non-resonant processes might be expected to be more significant for the photoexcitation of a nucleus as massive as that of ^{167}Er. Nevertheless, resonant absorption appears to be the dominant means of isomeric production for this nucleus as it was for the benchmark nuclide. The increase in normalized activation between the 4 and 6 MeV data strongly imply that a large gateway lies in this range. The magnitude of the data near 1.2 MeV suggests that a smaller activation edge lies below this energy. However, the small number of irradiations makes this assumption difficult to verify.

The measurements obtained from several nuclides, ^{77}Sr, ^{79}Br, ^{111}Cd, and ^{115}In did allow the identification of several resonances below 1.5 MeV. The integrated cross sections of these were found to be on the order of 1 to 10 $\times$ 10^{-29} cm^2-keV, and these results were reported previously.[7,8,11,12] A final isotope, ^{179}Hf, while not providing such detailed information, did indicate an activation edge at about 1.1 MeV for its isomer $^{179}Hf^m$ ($T_{1/2}$ = 18.68 sec). Its excitation function is displayed in Fig. 13 and again the relatively slow rise at high energies suggests resonant photoexcitation even for this large nucleus.

With the exceptions of ^{111}Cd, ^{77}Se, and ^{199}Hg, for which data are still being reduced, plots like those of Figs. 9, 12, and 13 for the remaining isotopes in Table I are qualitatively similar. Again, in the context of this study, primary importance is placed on the amount of variation occuring between different endpoint measurements since this may suggest the necessity of particular gateways. This information is given in Table II, in the form of $\sigma\Gamma$ values from Eq. (10). The fractional changes between 4 and 6 MeV measurements and between 6 and 10.4 MeV are also shown as κ_1 and κ_2, respectively.

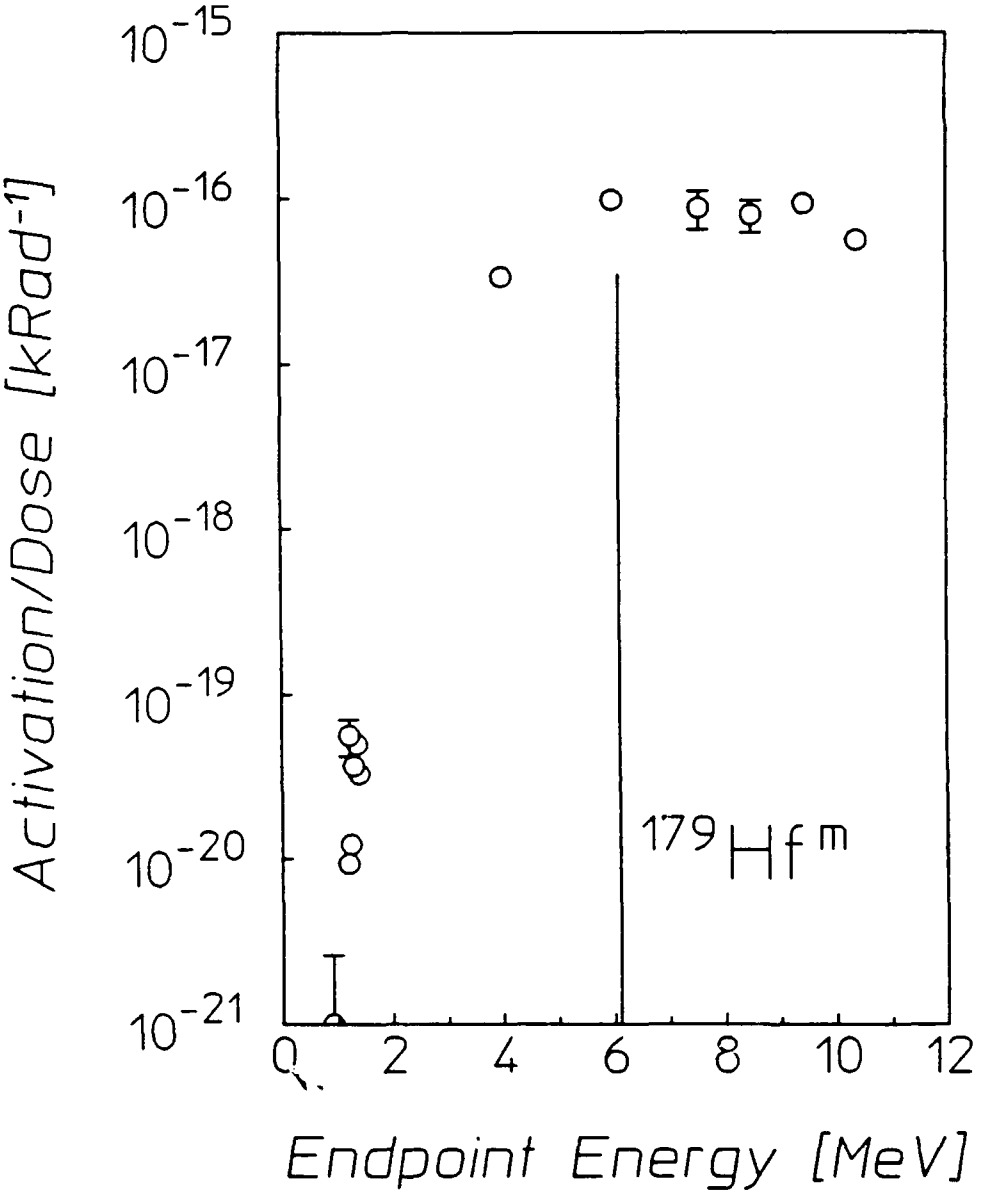

Figure 13: Normalized activation obtained from irradiations with all four accelerators for $^{179}Hf^{m}$ ($T_{1/2}$ = 18.68 sec). The size of the symbols is comparable to one standard deviation except where error bars are explicitly shown. The vertical line indicates the neutron evaporation threshold at E_n = 6.1 MeV.

Table II. Summary of experimental results. The quantity ΔJ is the change in spin between ground state and isomer. For both 4 and 6 MeV irradiations, the integrated cross sections of a single gateway state at the reference energy of 2.125 MeV are given as $(\sigma\Gamma)$ and have been corrected for thermal and epithermal neutron contaminations. The term "units" is used for the sake of brevity to represent units of 10^{-29} cm^2-keV. The ratio of 6 MeV values to those at 4 MeV are given as κ_1. The ratio of integrated cross sections obtained from 10.4 MeV to 6 MeV measurements is κ_2. Also given is the fraction of thermal and epithermal neutron contamination in the total activation, A_n/A_{Tot}. The comment NA is used in the column for A_n/A_{Tot} when no naturally abundant parent is available for (n,γ) reactions. An entry NA in the κ_2 column indicates that this information is not currently available.

Nuclide	ΔJ	4 MeV $(\sigma\Gamma)$ [units]	4 MeV A_n/A_{Tot} [%]	6 MeV $(\sigma\Gamma)$ [units]	6 MeV A_n/A_{Tot} [%]	κ_1	κ_2
^{167}Er	3	4600 ± 110	0.01	34000 ± 360	0.32	7.4	1.0
^{79}Br	3	660 ± 17	NA	1900 ± 23	NA	2.9	1.5
^{191}Ir	4	7600 ± 610	NA	36000 ± 960	NA	4.7	NA
^{197}Au	4	2600 ± 40	NA	13000 ± 64	NA	5.0	NA
^{89}Y	4	9 ± 5	NA	260 ± 8	NA	29	2.9
^{77}Se	3	330 ± 4	0.03	6500 ± 32	0.76	20	NA
^{179}Hf	4	9400 ± 120	0.04	25000 ± 110	6.41	2.7	1.1
^{137}Ba	4	330 ± 23	<0.01	1900 ± 23	0.07	5.8	1.4
^{199}Hg	6	260 ± 10	0.05	1400 ± 42	5.40	5.4	NA
^{111}Cd	5	920 ± 12	<0.01	2500 ± 44	0.07	2.7	NA
^{113}In	4	1300 ± 59	NA	4700 ± 180	NA	3.6	0.71
^{87}Sr	4	390 ± 13	<0.01	870 ± 18	0.89	2.2	2.3
^{176}Lu	6	14000 ± 95	0.01	35000 ± 2300	1.51	2.5	NA
^{115}In	4	1800 ± 16	NA	6700 ± 14	NA	3.7	1.5
^{180}Ta	8	18000 ± 6600	NA	35000 ± 650	NA	1.9	NA
^{135}Ba	4	1300 ± 62	<0.01	6000 ± 110	0.39	4.6	4.0
^{195}Pt	4	3000 ± 160	<0.01	14000 ± 220	0.03	4.7	NA
^{117}Sn	5	320 ± 47	<0.01	880 ± 26	0.07	2.8	0.84
^{123}Te	5	4200 ± 730	<0.01	6800 ± 320	1.45	1.6	NA

Figure 14 displays the effective integrated cross sections for $^{123}Te(\gamma,\gamma')^{123}Te^{m}$ reduced from 4 and 6 MeV measurements. This is the only isotope for which such curves clearly intersect at a location distinct from the 4 MeV asymptote. This plot suggests that normalized activations at both 4 and 6 MeV may have been produced by photoexcitation through the same gateway state near 3 MeV, with an integrated cross section on the order of 14000×10^{-29} cm^2-keV.

Neutron Excitations

All of the accelerators used, other than DNA/PITHON, were capable of evaporating neutrons from the operational environment. Since neutrons can also excite nuclei into their isomeric states it was important to determine the amount of normalized activation which was attributable to these particles. In principle, two types of neutron reactions could have occurred: inelistic (n,n') reactions which would have required hot neutrons and neutron capture (n,γ) processes driven by fluxes of thermal or epithermal neutrons. Both would have required a primary source of neutrons to have been active during the bremsstrahlung irradiation.

At the photon energies available to the medical linacs, only eight isotopes have thresholds for (γ,n) reactions. Four of these are unlikely and can be resonably excluded from consideration. The materials used in the irradiation devices and facility were documented, and in these only ^{2}H, ^{9}Be, ^{13}C, and ^{17}O were expected to serve as sources of neutrons in the linac environments.

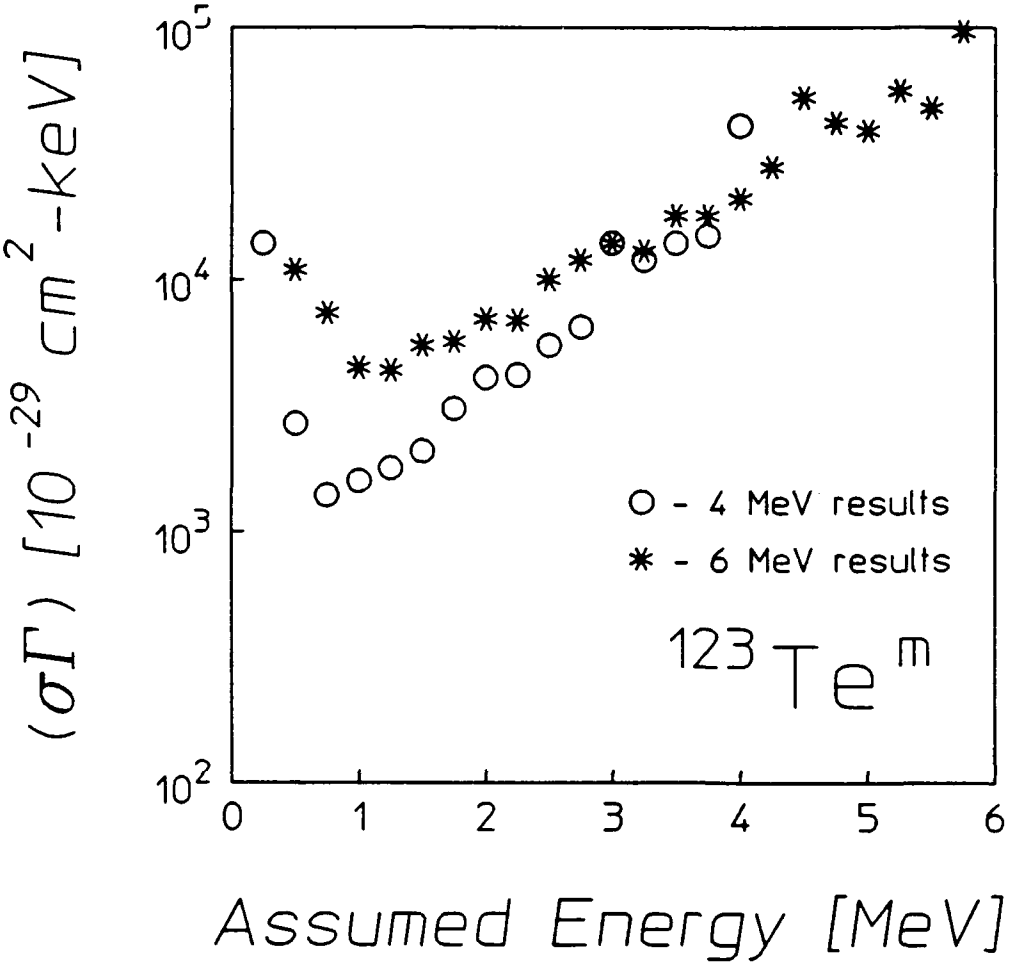

Figure 14: Integrated cross sections for the reaction $^{123}Te(\gamma,\gamma')^{123}Te^m$ through a single, unknown gateway state as a function of the energies at which this state could be assumed to lie. The circles indicate the results of measurements using the 4 MeV linac while the asterisks show those from the 6 MeV experiments.

The photon intensity was monitored throughout the course of these experiments, so the flux of primary photoneutrons could be calculated with reasonable accuracy from the following potential sources:

1.) a 0.025 cm thick Be window located below the bremsstrahlung converter target in the 6 MeV linac.

2.) the ^{2}H in the cooling water in the bremsstrahlung converter target.

3.) the ^{2}H in the humidity in the chamber and the ^{13}C and ^{17}O in the volume of atmosphere incidentally irradiated.

4.) the ^{2}H, ^{13}C and ^{17}O in the concrete used in construction.

Of these, the first dominated by orders-of-magnitude, giving an expected flux of 10^{3} neutrons/cm^{2}-sec at the position of the experimental samples.

The potential activation produced by such a flux is difficult to estimate because the cross sections for (n,n') reactions are poorly known. However, if it is assumed that all of the flux carries at least threshold energy, the cross section $\sigma_{n,100\%}$ necessary to produce all of the measured activation from neutrons can be calculated. These resulting values are summarized in Table III in units of barns and values can be seen to range from tens to thousands. This is to be compared with the few hundreds of millibarns that describe (n,n') reactions in those few cases where measurements have been reported in the literature.

Total neutron cross sections, which certainly must be greater than the inelastic component, are available for all of the materials studied.[22] They are summarized in Table III, together with any other cross sections which might bound more closely the value expected for relevant (n,n') reactions that might have contributed in producing the observed isomers.[23-30] Finally, in Table III is tabulated the ratio, Ω, which compares the most restrictive upper limit to $\sigma_{n,100\%}$, the cross section for inelastic neutron excitation which would be necessary to explain all of the observed yield.

Table III. Summary of fast neutron contamination limits for 6 MeV irradiations. The fast neutron cross section, $\sigma_{n,100\%}$ is that required to produce 100% of the observed activations. Maximum values for the true total neutron cross section of the element of interest,[25] σ_{tot}, are shown for the energy range 0.1 to 6 MeV. When available, the non-elastic cross section for the element has been shown in parentheses following the elastic cross section. The most restrictive additional cross section, σ_{lim}, for the particular isotope or element is given with its type and E_{max}, the energy up to which it was determined. Cross section types are as follows: ie = inelastic in element; i = inelastic in isotope; n = non-elastic in isotope; fi = inelastic in isotope, average for fission spectrum. The factor Ω is the ratio of the most specific observed cross section to the cross section required for a 100% contamination effect, and thus represents an upper limit for contamination of the neutron effects.

Nuclide	$\sigma_{n,100\%}$ [b]	σ_{tot} [b]	σ_{lim} [b]	Ref.	Type	E_{max} [MeV]	Ω [%]
^{167}Er	2700	9	-		-	-	0.33
^{79}Br	140	7.5	-		-	-	5.4
^{191}Ir	2590	10.3	-		-	-	0.40
^{197}Au	95	10	1.3	32	i	5.3	1.4
^{89}Y	20	11.5	0.2	27	i	4.0	1.0
^{77}Se	490	8.3(2.4)	0.73	26	fi	-	0.15
^{179}Hf	1940	20	0.4	31	i	1.6	0.02
^{199}Hg	120	10(2.6)	0.14	33	i	2.1	0.12
^{137}Ba	130	7.3(2)	0.66	30	i	3	0.51
^{111}Cd	210	8	0.23	26	fi	-	0.11
^{113}In	320	6.3	0.047	28	i	1.0	0.01
^{87}Sr	60	10	0.11	26	fi	-	0.18
^{176}Lu	2638	7	-		-	-	0.27
^{115}In	430	6.3	0.38	29	i	5.3	0.09
^{180}Ta	3016	8.5(2.9)	1.8	32	ie	1.8	0.06
^{135}Ba	420	7.3(2)	-		-	-	0.48
^{195}Pt	1350	10	0.68	32	ie	1.8	0.05
^{117}Sn	70	6.8(2)	-		-	-	2.9
^{123}Te	530	6	-		-	-	1.1

In effect Ω in Table III is the maximum fractional contamination through the fast neutron channel of the photoexcitation yield. As can be seen, values are generally smaller than 1% and exceptions occur only in cases for which restrictive estimates of (n.n') cross sections are unavailable. For those nuclides the only available values were those describing total processes which certainly bound the (n,n') reactions, but generously so. There is no reason to suspect that the unmeasured inelastic reactions are uniformly so large and that only the smallest appear in the literature. The best resolved are those limiting neutron contributions to a few tenths of a percent. It seems reasonable to conclude that in all cases examined in this work the (γ,γ') channels dominated over (n,n') by orders-of-magnitude for the linac irradiations.

The fast neutron flux expected in these experiments, 10^3 neutrons/cm^2-sec was too small to confirm by direct measurement at such high levels of irradiation. Nevertheless, in order to completely exclude the possibility of an undocumented emplacement of some strong photoneutron source such as ^{235}U in the irradiation environment, a measurement was attempted using standard procedures.[31,32] The (n,p) reactions of ^{46}Ti, ^{47}Ti, and ^{58}Ni are well-documented and provide clear signature photons for convenient periods of decay. These nuclei are not affected by the photon beam in this energy range but they are sensitive to fast neutrons, producing the daughters ^{46}Sc, ^{47}Sc, and ^{58}Co respectively.

In this measurement, the foils were irradiated, removed to the HPGe detector and counted to obtain pulse height spectra. In these spectra no signature photon peaks from the daughters were evidenced at any levels above the background of the counting chamber. It was therefore possible to obtain from this null result only an upper bound on the fast neutron flux at the sample position, which was 7×10^4 neutrons/cm^2-sec.

As can be seen, the limit established by measurement is not particlularly restrictive, being 70 times larger than the calculated values of fast neutron flux. Even if the limits of contamination in Table III are raised by this factor of 70, at least half of the samples would still be affected by errors of less than 10%. Only in the case of unknown inelastic cross sections for (n,n') reactions which closely approach the total values shown in Table III could an undocumented sample of rare material have produced a level of fast neutron flux sufficient to

contaminate the results of the (γ,γ') reactions being studied. Such occurrences would have required the coincidence of very improbable circumstances and merit no further consideration. That so little fast neutron contamination occurred from use of the 6 MeV linac precluded any possibility of significant effects of fast neutrons in the 4 MeV experiments.

Contributions to the observed activations from (n,γ) reactions could be directly determined. The thermal and epithermal neutron fluxes due to the 6 MeV linac, Φ_{th} and Φ_{ep}, were measured in that environment by irradiating two thin indium foils, one of which was shielded from thermal neutrons by a cadmium cover. In accordance with standard techniques,[33] energy spectra obtained from these foils were examined after exposure for signature photons from the isomer $^{116}In^{m}$, which is produced by a branch of the reaction $^{115}In(n,\gamma)^{116}In^{m,g}$. The magnitudes of the fluorescence lines observed in both the bare and the shielded samples allowed the determination of the neutron fluxes Φ_{th} = 12 neutrons/cm^2-sec and Φ_{ep} = 6 neutrons/cm^2-sec from literature values of the thermal and epithermal neutron cross sections.[34] The neutron fluxes from the 4 MeV linac were bounded in a similar way. A bare indium foil was exposed, but later showed no photopeaks from $^{116}In^{m}$ above the background. Upper bounds for the neutron fluxes were found by assuming for the 4 MeV environment the same 2:1 ratio of thermal to epithermal neutrons found at 6 MeV. The activation was taken to be just below the level of noise and gave $\Phi_{th} \leq 6$ neutrons/cm^2-min and $\Phi_{ep} \leq 3$ neutrons/cm^2-min during operation of the 4 MeV linac. The small amount of activation of each of the isomers due to these neutrons was subtracted from the total activation observed. In no case did the contribution from thermal and epithermal neutrons in the 4 MeV environment exceed 0.05%. The thermal and epithermal neutron fluxes in the 6 MeV chamber produced contributions below 1.5% for all isomers except for $^{179}Hf^{m}$ (6.4%) and $^{199}Hg^{m}$ (5.4%). Even in these materials, it is apparant that photoexcitation was the dominant mechanism for the observed activation. The contributions to the activation from thermal and epithermal neutrons is summarized in Table II for each of the 19 nuclides studied.

In the DNA/Aurora environment the target chamber consisted of a large concrete room in which the most intense and high energy photons propagated in an essentially horizontal direction.[35,36] The most intense spot was centered at about 30 cm from the face of the machine, and was located approximately 1.2 meters above the floor of the 5 meter high

chamber. The wall towards which the beam was directed was 19.5 meters away from the sample position. This geometry contributed two factors of importance. First, if fast neutrons were produced by (γ,n) reactions in the bremsstrahlung field, the lack of dense moderators near the samples made it unlikely that a significant thermal or epithermal neutron flux was present. Second, of the materials within the target chamber only ^{2}H, ^{17}O, ^{13}C, and ^{181}Ta were likely neutron sources since their neutron binding energies are less than the maximum photon energy produced by the accelerator, about 11 MeV. Clearly the most probable source of fast neutrons in the target chamber was the tantalum, with a neutron binding energy of 7.61 MeV. This assumption allowed the maximum neutron energies to be found from the endpoint energies of the bremsstrahlung produced at different charge voltages. Table IV lists these values.

A determination of the slow neutron flux was made by examining the energy spectra of samples containing natural abundances of the isotopes ^{197}Au and ^{115}In. These nuclei are susceptible to the capture of thermal and epithermal neutrons and produce the daughter nuclei ^{198}Au and ^{116}In, whose decays are marked by distinct signature lines. The spectra of the gold samples showed no evidence of full energy peaks above the level of the background at the fluorescence energies of either the ground or isomeric states of ^{198}Au. On the other hand, spectra of indium samples obtained following shots at 100 kV charge voltage did contain very small peaks at the fluorescence energy of 1097.29 keV from the decay of $^{116}In^{m}$ ($T_{1/2}$ = 54.15 min). The numbers of counts in these peaks were used to calculate the normalized activation of this species for 100 kV shots and the slow neutron flux which corresponded to this amount of excitation, Φ_{slow} = (1680 ± 310) neutrons/cm^2-krad. The latter calculation was made by using the thermal neutron cross section rather than the larger epithermal resonance integral.[34] This was done in order to achieve an upper bound on the number of slow neutrons since it was not possible to determine the proportions of thermal to epithermal neutrons from the targets exposed.

Table IV. Summary of various energy parameters estimated for the charge voltages employed in these experiments. The values given for E_{end} are the approximate endpoint energies of the bremsstrahlung produced by DNA/Aurora. The quantity E_{max} indicates the maximum possible energy for neutrons produced through (γ,n) reactions.

Charge Voltage [kV]	E_{end} [MeV]	E_{max} [MeV]
70	6.61	0.00
80	7.56	0.00
90	8.50	0.89
100	9.44	1.83
110	10.39	2.78
115	10.86	3.25
118	11.14	3.53

The projected number of slow neutrons produced during a 118 kV shot was found by scaling the 100 kV value by a factor of 1.92 which represented the rise in maximum neutron energy between these charges. The slow neutron flux for the 118 kV shot was determined to have been (3240 ± 610) neutrons/cm^2-krad. The measurements of photoexcitation for the nuclei ^{79}Br, ^{89}Y, ^{113}In, ^{115}In, and ^{180}Ta were free from slow neutron contamination since there are no naturally abundant parents for (γ,n) reactions.[37] The largest neutron capture cross section for the production of the remaining isotopes in Table I is 100 barns,[34] the resonance cross section for ^{167}Er, and therefore at the highest charge voltage the amount of isomeric activation due to slow neutrons was only 3.24×10^{-19} krad^{-1}. Thus even in the most critical case, less than 1% of the total activation, on the order of 10^{-16} krad^{-1}, was provided by slow neutrons.

The number of fast neutrons produced in the target chamber was found in a similar way. Spectra of samples which contained natural abundances of ^{80}Se, ^{82}Se, ^{109}Ag, and ^{116}Cd were examined for any sign of the decay signatures of the daughter nuclei ^{80}As, ^{82}As, ^{109}Pd, and ^{116}Ag which are produced by (n,p) reactions. No such signatures were found above the background level. Nevertheless, it was possible to obtain an upper bound on the numbers of each daughter produced by considering the maximum size of a fluorescence peak which could be hidden by statistical fluctuations of the background. The (n,p) reaction cross sections[22] appropriate to the maximum neutron energies were then used to determine upper bounds on the fast neutron flux. When the scaling of the maximum neutron energies was taken into account, the most restrictive upper bound was obtained for the reactions ^{80}Se(n,p)^{80}As and ^{82}Se(n,p)^{82}As at 100 kV. The fast neutron flux at this charge was found to be Φ_{Fast} = (2090 ± 660) neutrons/cm^2-krad. The number of fast neutrons scaled to 118 kV was then (2660 ± 840) neutrons/cm^2-krad. The largest fast neutron cross section for the elements examined in these experiments are on the order of tens of barns, values much greater than the inelastic cross sections for the particular isotopes in question. The amount of fast neutron activation of these nuclei was therefore on the order of 10^{-20} krad^{-1}, and again the neutron contamination was negligible.

CONCLUSIONS

The principal conclusion of this work is that a combination of technical and computational advances has made possible the study of (γ,γ') reactions with greater precision than had been possible in the classical works appearing in the literature. The pernicious lack of convergence of those earlier measurements is now understood to have been a consequence of unexpected intensities of continua in the spectra of the photon sources being used. The results reported here show that when the most current technology is applied to the characterization of the irradiations, the amounts of activation achieved with different accelerators are consistent. Moreover, in the uncontested case[18] of the reaction $^{87}Sr(\gamma,\gamma')^{87}Sr^{m}$ the current results from the four accelerators are in complete agreement with the literature.

This reaction for the photoexcitation of $^{87}Sr^{m}$ is particularly important as a benchmark. Up to a bremsstrahlung endpoint energy of 4 MeV, the activations produced in the strontium samples were completely consistent with the 1967 measurements[18] of three gateways at 1.22, 1.88, and 2.66 MeV. This was shown in Fig. 11a. As seen in Fig. 11b, *only one additional gateway was needed between 4 and 6 MeV to explain all of the remainder of the data up to 11 MeV.*

Since the density of excited states increases exponentially with excitation energy, it might have been reasonably expected that the number of gateway states for the photoexcitation of isomers would also increase to very high values. However, such a possibility does not seem to be supported by the data obtained in our experiments, as typified in Figs. 9 and 11a. There seems to be a discrete state or compact band of states in the 4 to 11 MeV range contributing the single jump in activation observed between 4 and 6 MeV. A phenomenon so localized in energy can be usefully described in terms of an effective integrated cross section, $\sigma\Gamma$, for the photoexcitation of isomers, as was defined in Eq. (10). Of course, for a nuclide such as ^{87}Sr where there are two major gateways, the value of $\sigma\Gamma$ obtained with bremsstrahlung having an endpoint energy great enough to excite both will be larger than what would be measured with bremsstrahlung able to excite only one. Just this result is seen in Table II for ^{87}Sr, as well as for several other nuclides.

The most surprising conclusions of this work is that some of the integrated cross sections for exciting isomers are extraordinarily large, approaching 10^{-21} cm^2-eV. Typified by the reaction $^{167}Er(\gamma,\gamma')^{167}Er^m$, these also seem to occur through discrete gateways or through narrow bands of gateway states. The data of Fig. 12 has a compelling resemblance to that for the excitation of one of the gateways in ^{87}Sr. The same sharp jump in activation with increasing x-ray endpoint is followed by relatively level yield up to 11 MeV. It is possible to fit the data of Fig. 12 with a single gateway near 4 MeV but more detailed considerations suggest there are two gateways in ^{167}Er. On the other hand, the excitation function for the reaction $^{179}Hf(\gamma,\gamma')^{179}Hf^m$ shown in Fig. 13 seems compelling in suggesting a single jump in activation at energies below 4 MeV.

Figures 10 and 14 show plots of the integrated cross sections of single gateway states as functions of the energies at which they might lie as found in both 4 and 6 MeV linac experiments. An examination of these graphs reveals the interesting feature that the 4 and 6 MeV curves intersect. The curves must always cross at some energy less than or equal to 4 MeV since each is generated in part by inverting the function F(E). Whenever the crossing point falls at 4 MeV, this behavior is simply due to the linear independence of the two irradiating spectra: above 4 MeV, F(E) is zero for the output of the 4 MeV linac while F(E) is non-zero for the 6 MeV spectrum. This provides an asymptote at 4 MeV for curves generated for all isotopes. However, in cases where the intersection point lies below 4 MeV some information regarding the location of a dominant gateway may be inferred. Assuming, for example, that photoexcitation in some nuclide is dominated by a single gateway at 2.5 MeV for photon energies up to 6 MeV, the 4 and 6 MeV integrated cross section curves will become equal near 2.5 MeV. The appearance of such a crossing in the results of experimental observations can be due to other factors, but in some instances may suggest the location of a single, dominant resonant state.

All of the materials studied show some variation in the location of the intersection point, but most lie close to 4 MeV as in the case of ^{167}Er. These likely convey no information about the energy of a dominant gateway. The lowest energy for such a crossing occurs for production of the isomer $^{123}Te^m$. Examination of Fig. 14 shows that the integrated cross section curves become equal in the vicinity of 3 MeV. This would imply the existence of a single mediating level having an integrated

cross section of 14000 × 10^{-29} cm^2-keV. If this is indeed the case, $^{123}Te^m$ may form the cornerstone of an extension of the spectral calibration technique used in Refs. 7 and 8 for energies up to 6 MeV.

Of the nuclides examined in this work, those most likely to have single gateway states are those which had the smallest increases in activation in changing from 4 MeV bremsstrahlung to 6 MeV. The ratios of values of ($\sigma\Gamma$) which determine the activations with 6 MeV endpoints to those from 4 MeV endpoints are shown in Table II as κ_1. The smaller values represent the behaviors seen in Fig. 14 that suggests single gateway states.

The difficulties in explaining the sizes of the integrated cross sections reported in this work accrue from the large changes in angular momentum, J separating ground states from isomers. Most of the larger values belong to nuclei which are spheroidal and the projections of angular momentum, K, upon the axes of elongation further inflame the difficulties. With an absorption transition of reasonable probability changes in J and K are limited to $\Delta J \leq 2$ and $\Delta K \leq 2$. While the first might be satisfied by making a transition from the ground state to a high member of a rotational band built upon the final state, the second would be violated because K is conserved within a rotational band. What is needed is a mechanism to mix K values of nuclear levels belonging to rotational bands built upon initial and final states of the (γ,γ') reaction.

It is interesting to speculate that this might occur as a result of couplings to states built upon cores of non-fissioning shape isomers.[38] Such states show double minima in energy as functions of elongation, even at low values of spin. At some values of excitation energy the shape of such a nucleus would be unstable and projections upon its principal axes would no longer be conserved. In this way the transition from a K value characteristic of the ground state to one consistent with the isomer might occur by mixing with such a state. In any case the pervasiveness found for the giant values of integrated cross sections for photoexcitation found in this work argues for some type of core property varying slowly with increasing nuclear size. Further work is needed to resolve the precise cause of this phenomenon.

REFERENCES

1. See for example the review, S. S. Dietrich and B. L. Berman, At. Data and Nuc. Data Tables 38, 199 (1988).

2. B. Pontecorvo and A. Lazard, C. R. Acad. Sci. 208, 99 (1939).

3. G. B. Collins, B. Waldman, E. M. Stubblefield and M. Goldhaber, Phys. Rev. 55, 507 (1939).

4. Y. Watanabe and T. Mukoyama, Bull. Inst. Chem. Res. 57, 72 (1979).

5. M. Krcmar, A. Ljubicic, K. Pisk, B. Logan and M. Vrtar, Phys. Rev. C 25, 2097 (1982).

6. I. Bikit, J. Slivka, I. V. Anicin, L. Marinkov, A. Ruydic and W. D. Hamilton, Phys. Rev. C 35, 1943 (1987).

7. J. A. Anderson and C. B. Collins, Rev. Sci. Instrum. 58, 2157 (1987).

8. J. A. Anderson and C. B. Collins, Rev. Sci. Instrum. 59, 414 (1988).

9. *The EGS4 Code System*, Walter R. Nelson, Hideo Hirayama and David W. O. Rogers, SLAC Report 265 (Stanford Linear Accelerator Center, Stanford, Calif. 1985).

10. *ITS: The Integrated TIGER Series of Coupled Electron/Photon Monte Carlo Transport Codes*, J. A. Halbleib and T. A. Mehlhorn, Sandia National Laboratories, SAND84-0573 (1984).

11. J. A. Anderson, M. J. Byrd and C. B. Collins, Phys. Rev. C 38, 2838 (1988).

12. C. B. Collins, J. A. Anderson, Y. Paiss, C. D. Eberhard, R. J. Peterson and W. L. Hodge, Phys. Rev. C 38, 1852 (1988).

13. *Evaluated Nuclear Structure Data File* (Brookhaven National Laboratory, Upton, New York, 1986).

14. C. B. Collins, C. D. Eberhard, J. W. Glesener and J. A. Anderson, Phys. Rev. C 37, 2267 (1988).

15. A. G. W. Cameron, in *Essays in Nuclear Astrophysics*, edited by C. A. Barnes, D. D. Clayton and D. N. Schramm (Cambridge, Univ. Press, Cambridge, 1982), p. 23.

16. A. Richter and W. Ziegler, Private communication.

17. J. J. Carroll, J. A. Anderson, J. W. Glesener, C. D. Eberhard, and C. B. Collins, Astrophys. J. 344, 454 (1989).

18. E. C. Booth and J. Brownson, Nucl. Phys. A98, 529 (1967).

19. E. Browne and R. B. Firestone, *Table of Radioactive Isotopes*, edited by V. S. Shirley (Wiley, New York, 1986).

20. B. Bernstein and I. B. Smith, IEEE Trans. Nucl. Sci. NS-20, 294 (1973).

21. R. Mohan, C. Chui and L. Lidofsky, Med. Phys. 12, 595 (1985).

22. *Neutron Cross Sections: Volume II, Curves*, Third Edition, D. I. Garber and R. R. Kinsey, BNL 325 (National Neutron Cross Section Center, Brookhaven National Laboratory, Upton, New York, 1976).

23. A. Calamand, "Cross Sections for Fission Neutron Spectrum Induced Reactions" in *Handbook of Nuclear Activation Cross Sections*, International Atomic Energy Agency Technical Report Series No. 156 (IAEA, Vienna, 1974).

24. E. Ramstrom, Nucl. Phys. A315, 143 (1979).

25. H. A. Grench and H. O. Menlove, Phys. Rev. 165, 165 (1968).

26. H. C. Martin, B. C. Diven and R. F. Taschek, Phys. Rev. 93, 199 (1954).

27. C. P. Swann and F. R. Metzger, Phys. Rev. 100, 1329 (1955).

28. G. L. Sherwood, A. B. Smith and J. G. Whalen, Nucl. Sci. & Eng. 39, 67 (1970).

29. J. B. Guernsey and A. Wattenberg, Phys. Rev. 101, 1516 (1956).

30. K. Sakurai and I. Kondo, Nucl. Inst. and Meth. 187, 649 (1981).

31. *ASTM Standard Method for Determining Neutron Flux, Fluence and Spectra by Radioactivation Techniques*, Publication E 261-77 (American Society for Testing and Materials, Philadelphia, 1987), and references cited there.

32. K. H. Beckurts and K. Wirtz, *Neutron Physics*, Trans. by L. Dresner (Springer-Verlag, New York, 1964).

33. *ASTM Standard Method for Determining Thermal Neutron Reaction and Fluence Rates by Radioactivation Techniques*, Publication E 262-86 (American Society for Testing and Materials, Philadelphia, 1987) and references cited there.

34. *Chart of the Nuclides*, Thirteenth Edition, F. W. Walker, D. G. Miller, and F. Feiner, Eds. (General Electric Company, San Jose, Calif. 1983).

35. *The Aurora Bremsstahlung Environment*, K. G. Kerris, Harry Diamond Laboratories Report No. HDL-TM-81-18, Harry Diamond Laboatories, 1981 (unpublished).

36. *Aurora User Guide*, Harry Diamond Laboratories, 1987 (unpublished).

37. *Nuclear Wallet Cards*, J. K. Tuli, (National Nuclear Data Center, Brookhaven National Laboratory, 1985).

38. M. Girod, J. P. Delaroche, D. Gogny, and J. F. Berger, Phys. Rev. Lett. 62, 2452 (1989).